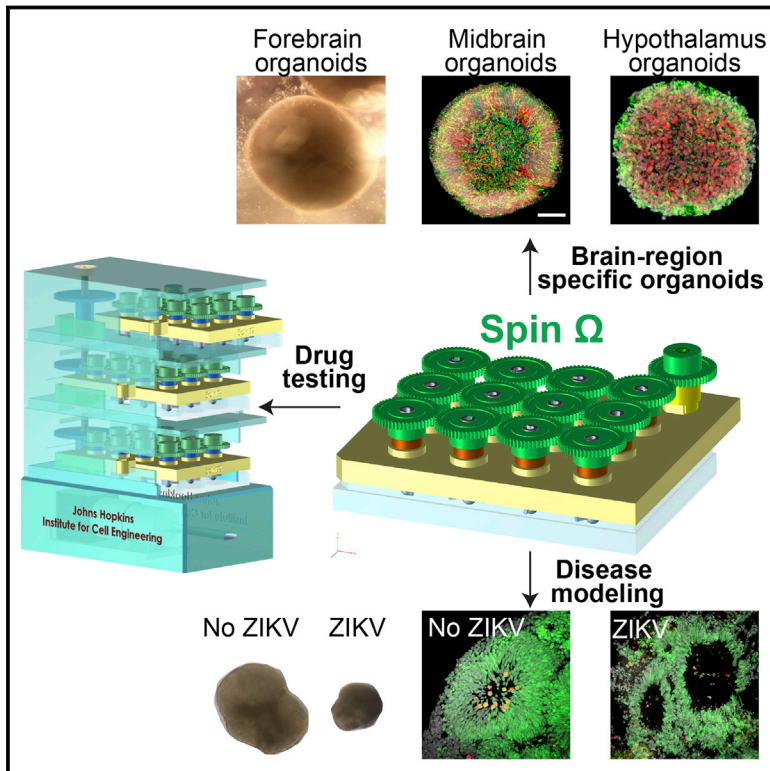# Cell

Brain-Region-Specific Organoids Using Mini-bioreactors for Modeling ZIKV Exposure

Graphical Abstract

Authors

Xuyu Qian, Ha Nam Nguyen, Mingxi M. Song, ..., Hengli Tang, Hongjun Song, Guo-li Ming

Correspondence

shongju1@jhmi.edu (H.S.), gming1@jhmi.edu (G.-l.M.)

In Brief

Zika virus preferentially infects neural progenitors in early stage cortical organoids generated using cost-effective miniaturized spinning bioreactors, resulting in suppressed proliferation, increased cell death, and macroscopic features resembling microcephaly.

Highlights

- A miniaturized spinning bioreactor for cost-effective culturing of organoids

- Generation of brain-region-specific organoids from human iPSCs

- ZIKV causes decrease of neuronal cell-layer volume resembling microcephaly

- Both African and Asian ZIKV infect neural progenitors in organoids

Accession Numbers

GSE80073

CellPress

Resource

Brain-Region-Specific Organoids Using Mini-bioreactors for Modeling ZIKV Exposure

Xuyu Qian,[1,2,18] Ha Nam Nguyen,[1,3,4,18] Mingxi M. Song,[1,9] Christopher Hadiono,[1,10] Sarah C. Ogden,[11]
Christy Hammack,[11] Bing Yao,[12] Gregory R. Hamersky,[5] Fadi Jacob,[1] Chun Zhong,[1,4] Ki-jun Yoon,[1,4] William Jeang,[1,14]
Li Lin,[12] Yujing Li,[12] Jai Thakor,[1] Daniel A. Berg,[1] Ce Zhang,[1,4] Eunchai Kang,[1,4] Michael Chickering,[1] David Nauen,[1,6]
Cheng-Ying Ho,[15,16] Zhexing Wen,[1,4] Kimberly M. Christian,[1,4] Pei-Yong Shi,[17] Brady J. Maher,[5,7] Hao Wu,[13] Peng Jin,[12]
Hengli Tang,[11] Hongjun Song,[1,3,4,8,*] and Guo-li Ming[1,3,4,7,8,*]
[1]Institute for Cell Engineering
[2]Biomedical Engineering Graduate Program
[3]Graduate Program in Cellular and Molecular Medicine
[4]Department of Neurology
[5]Lieber Institute for Brain Development
[6]Department of Pathology
[7]Department of Psychiatry and Behavioral Sciences
[8]The Solomon Snyder Department of Neuroscience
Johns Hopkins University School of Medicine, Baltimore, MD 21205, USA
[9]Riverhill High School, Clarksville, MD 21029, USA
[10]Byram Hills High School, Armonk, NY 10504, USA
[11]Department of Biological Science, Florida State University, Tallahassee, FL 32306, USA
[12]Department of Human Genetics, School of Medicine
[13]Department of Biostatistics and Bioinformatics, Rollins School of Public Health
Emory University, Atlanta, GA 30322, USA
[14]Clear Lake High School, Harris, TX 77058, USA
[15]Division of Pathology, Children's National Medical Center
[16]Pathology and Pediatrics
George Washington University, Washington, DC 20010, USA
[17]Department of Biochemistry and Molecular Biology, Sealy Center for Structural Biology and Molecular Biophysics, University of Texas
Medical Branch, Galveston, TX 77555, USA
[18]Co-first authors
*Correspondence: shongju1@jhmi.edu (H.S.), gming1@jhmi.edu (G.-l.M.)
http://dx.doi.org/10.1016/j.cell.2016.04.032

SUMMARY

Cerebral organoids, three-dimensional cultures that model organogenesis, provide a new platform to investigate human brain development. High cost, variability, and tissue heterogeneity limit their broad applications. Here, we developed a miniaturized spinning bioreactor (SpinΩ) to generate forebrain-specific organoids from human iPSCs. These organoids recapitulate key features of human cortical development, including progenitor zone organization, neurogenesis, gene expression, and, notably, a distinct human-specific outer radial glia cell layer. We also developed protocols for midbrain and hypothalamic organoids. Finally, we employed the forebrain organoid platform to model Zika virus (ZIKV) exposure. Quantitative analyses revealed preferential, productive infection of neural progenitors with either African or Asian ZIKV strains. ZIKV infection leads to increased cell death and reduced proliferation, resulting in decreased neuronal cell-layer volume resembling microcephaly. Together, our brain-region-specific organoids and SpinΩ provide an accessible and versatile platform for modeling human brain development and disease and for compound testing, including potential ZIKV antiviral drugs.

INTRODUCTION

Human-induced pluripotent stem cells (iPSCs) can generate virtually any cell type in the body to model human development and disease, screen for therapeutic drugs, and develop cell-replacement therapies. Traditional monolayer cultures allow for external control of targeted differentiation of human iPSCs to produce more uniform cell populations; however, these cultures lack 3D cell assembly properties that define endogenous biological systems. Structures resembling whole developing organs, named organoids, have recently been generated via 3D cultures and include intestinal, kidney, retinal, and cerebral organoids (Lancaster and Knoblich, 2014; Yin et al., 2016). Organoid technology evolved from embryoid body cultures, which are 3D aggregates of stem cells that self-organize to develop disparate tissues in vitro, similar to teratoma formation in vivo. Organoids provide a unique opportunity to model human organogenesis, which is not accessible to experimentation. An immediate

Cell

application of organoid technology would be to address the current global public health emergency concerning a suspected link between Zika virus (ZIKV) and microcephaly, a neurodevelopmental disorder, by modeling human brain development.

One recent advance in cerebral organoid technology was the adoption of a spinning bioreactor to facilitate nutrient and oxygen absorption, which enables formation of longer neuroepithelium-like zones and supports growth of large, complex organoids that more closely resemble the developing human brain than had been achieved by previous approaches (Lancaster et al., 2013). Derived from an early NASA-designed rotating wall vessel bioreactor to simulate microgravity, this technology potentially offers two additional benefits: (1) low fluid shear stress to promote cell-cell interactions and induction of differentiation (Goodwin et al., 1993) and (2) randomized gravitational vectors that affect intracellular signal transduction and gene expression (Jessup et al., 1993). This and other human cerebral organoid technologies (Kadoshima et al., 2013; Lancaster et al., 2013; Mariani et al., 2015; Muguruma et al., 2015; Paşca et al., 2015) have generated much excitement for using organoids to model human brain development and disorders.

Despite the promise of these pioneering organoid technologies, there are several major challenges. First, available spinning bioreactors require a large volume of medium and incubator space (Figure S1Aa). With frequent media changes over several months of culturing, the system is cost prohibitive for most laboratories and precludes scalability, use of growth factors, or chemical screening. It also presents a roadblock for testing different conditions to optimize protocols. Second, the current cerebral organoid methodology ("intrinsic protocol") is based on cell self-assembly without external control, and thus each organoid is typically comprised of diverse cell types found in forebrain, hindbrain, and retina (Lancaster et al., 2013). Large sample-to-sample variability associated with current methods complicates quantitative analyses and limits applicability. Third, key features of human brain development have yet to be robustly recapitulated in cerebral organoids. For example, unlike rodents, the embryonic human cerebral cortex contains an abundant population of specialized outer radial glia cells (oRGCs) in the outer subventricular zone (oSVZ), the cellular population considered pivotal to the evolutionary increase in human cortex size and complexity (Lui et al., 2011). Current cerebral organoids contain only sparse progenitors that have morphological characteristics of oRGCs, and none have exhibited a well-developed oSVZ layer. Taken together, there is a critical need to develop an organoid platform with reduced cost, higher throughput, and increased reproducibility and one that better resembles critical aspects of human cortical development.

To address these challenges, we engineered a miniaturized spinning bioreactor using 3D design and printing technology and developed a protocol to generate forebrain-specific organoids from human iPSCs, which recapitulate human embryonic cortical development in a reproducible and quantifiable manner. We also developed protocols for midbrain and hypothalamic organoids. For proof-of-principle applications of our platform, we performed chemical compound testing and modeled ZIKV exposure. Our versatile, simple-to-use, cost-effective, and reproducible brain-region-specific organoid platform provides accessible

and affordable technology to a broad scientific community for modeling human organogenesis and human disorders and for compound testing.

RESULTS

A Miniaturized Spinning Bioreactor to Optimize Organoid Cultures

To reduce the cost of generating organoids under different conditions, we attempted to miniaturize the large spinning flask. Nonlinear fluid dynamics precluded simply scaling down the system. Instead, we engineered a multi-well spinning device to fit a standard 12-well tissue culture plate. Above the cover, spinning shafts are attached to a set of 13 interconnecting gears, driven by a single electric motor (Figure 1A). We used computer-aided design software to design and 3D print each component. We assembled prototypes to optimize designs that sustain organoids of varying sizes in suspension under moderate spinning speed and prevent aggregation at the center of each well. After multiple rounds of systematic optimization of individual components, including number, shape, size, and angle of leafs and diameter, length, and shape of shafts, we arrived at SpinΩ, a miniaturized spinning bioreactor unit that requires as little as 2 ml of media per well, a 50-fold reduction in media consumption, and drastically reduced incubator space (Figure S1Ab). We further designed a modular stackable version with insertable cassettes driven by one common motor (Figure S1Ac). The miniaturized spinning bioreactor permits comparisons of a large number of conditions in parallel for protocol optimization.

To reduce tissue heterogeneity, we pre-patterned embryoid bodies to the fate of a specific brain region. We first treated human iPSCs with dual SMAD inhibitors (dorsomorphin and A-83) for 7 days and then embedded embryoid bodies in Matrigel for another 7 days, followed by Matrigel removal and spinning in SpinΩ (Figure 1B). Compared to the "intrinsic protocol," we could reliably generate organoids from multiple iPSC lines with reduced heterogeneity in organoid shape and size (Figures S1B and S1C). However, there was significant cell death within organoids, as shown by activated caspase-3 (CAS3) immunostaining (Figures S1D and S1E and Table S1). We then tested combinations of different signaling molecules for various durations. We found that treatment with three factors, GSK-3β inhibitor CHIR99021, recombinant WNT3A protein, and SMAD inhibitor SB-431542, during the Matrigel stage drastically reduced the number of CAS3$^+$ cells at day 14 (Figures S1D and S1E). Later, we determined that the WNT3A contribution was minimal, likely because WNT3A and CHIR99021 activate the same downstream signaling pathway (Figures S1D–S1F). At day 14, well-defined polarized neuroepithelium-like structures resembled neural tubes, with a nearly pure population of NESTIN$^+$ SOX2$^+$ NPCs and expression of adherent junction markers (β-CATENIN and PKCλ) and proliferation marker phosphohistone H3 (PH3) near the ventricular surface (Figures 1C and S1F). Notably, individual neuroepithelium-like structures were consistently much larger than those generated without treatment of these factors (Figure S1D). Upon spinning in SpinΩ, organoids developed into multi-layer stratified structures, composed of SOX2$^+$ NPCs, TBR2$^+$ intermediate progenitor cells (IPCs), and
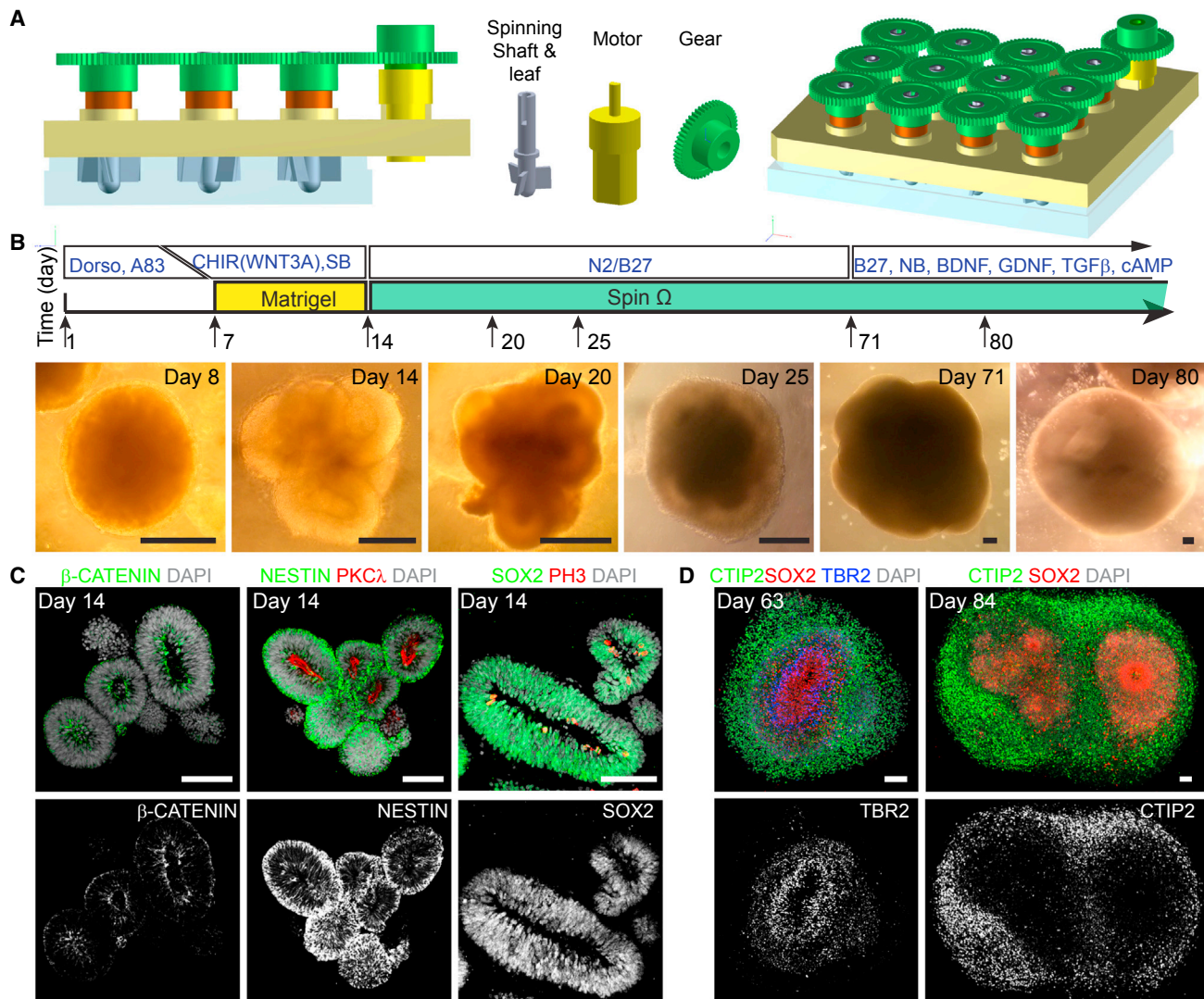
Figure 1. SpinΩ Bioreactor-based Forebrain Organoid Culture System

(A) Computer-aided design drawings of 12-well version SpinΩ bioreactor and individual parts.

(B) Schematic diagram of forebrain organoid protocol and sample phase images at different stages. Scale bars, 200 μm.

(C and D) Immunostaining of forebrain organoids at days 14, 63, and 84 (tiling image). Scale bars, 100 μm.

Also see Figure S1 and Table S1.

CTIP2$^+$ neurons (Figure 1D). With a small volume, it became affordable to supplement media with growth factors at later stages (Figure 1B).

In comparison, we maintained organoids in stationary cultures after day 14. At day 42, there was substantial cell death in the interior (Figure S1G). Ventricular structures were largely absent; instead, extensive neurogenesis without defined organization was observed (Figure S1H). We also cultured forebrain organoids using orbital shakers under a similar rotation speed as spinning in SpinΩ. At day 42, organoids showed substantial cell death in the neuronal layer despite retaining defined ventricular structures (Figure S1I). These results suggest that spinning cultures enhance cell viability and promote maintenance of the stem cell niche, at least for forebrain organoids generated using

our protocol. The miniaturized spinning bioreactor platform opens doors for cost-effective generation of organoids and provides accessible and affordable organoid technology to a broader scientific community.

Organoids with a Forebrain Identity and Increased Homogeneity

We next performed detailed characterizations of early stage forebrain organoids (Figure 1B). At day 14, immunohistological analysis showed almost exclusive expression of forebrain-specific progenitor markers, including PAX6, OTX2, and FOXG1, with minimal expression of markers for other brain regions tested (Figures 2A and S2A). We obtained similar results with multiple iPSC lines and with different clones (Figures 2A, S2A, and

(legend on next page)

Cell
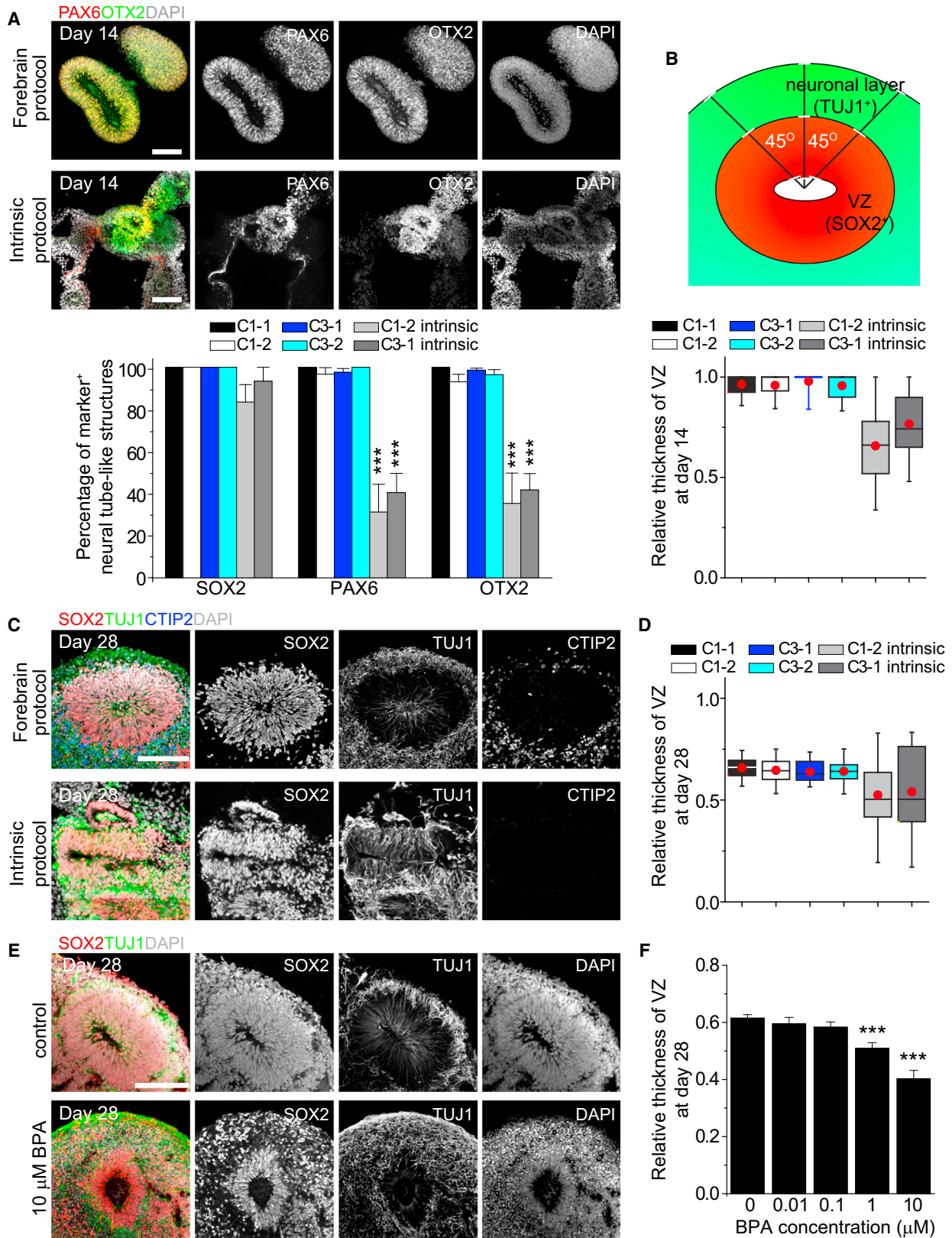
S2B). Consistent with previous findings, cerebral organoids generated in large spinning flasks using the "intrinsic protocol" exhibited diverse brain region identities with fewer than 50% of rosettes expressing PAX6 or OTX2 (Figures 2A, S2A, and S2B).

We further assessed the temporal consistency of neuronal differentiation by quantifying the relative thickness of SOX2$^+$ ventricular zone-like (VZ) layer and TUJ1$^+$ neuronal layer between apical and basal surfaces at specific time points (Figure 2B). At day 14, organoids generated using the "intrinsic protocol" exhibited varying degrees of neurogenesis with mixed cell types, whereas very few TUJ1$^+$ neurons were detected in forebrain organoids (Figure S2A). As a result, our protocol produced organoids with nearly all cells organized in the VZ layer at this stage (Figure 2B). By day 28, we observed a consistent ratio between SOX2$^+$ progenitor layer and TUJ1$^+$/CTIP2$^+$ neuronal layer in forebrain organoids, compared to the large variability using the "intrinsic protocol" (Figures 2C and 2D).

The apparent homogeneity of forebrain organoids, small volume per condition, and multi-well format of SpinΩ comprise a platform that is amenable to chemical compound testing. As a proof of principle, we tested the effect of Bisphenol A (BPA), which is commonly found in household plastic products and is known to affect rodent neural development (Kundakovic et al., 2013). Treatment of forebrain organoids from days 14 to 28 with BPA led to a dose-dependent decrease in the relative VZ thickness at day 28 (Figures 2E and 2F). With acute treatment of higher BPA concentrations for 24 hr and then pulse-labeling proliferating cells with EdU (Figure S2C), quantitative analysis showed decreased density of EdU$^+$ or PH3$^+$ NPCs (Figures S2D and S2E), indicating that reduced NPC proliferation contributes to decreased relative VZ thickness.

Multiple Progenitor Zones Recapitulating Human Embryonic Cortical Development

To characterize developmental dynamics, we systematically performed immunohistochemical analyses of day 28, 56, and 84 organoids. We observed well-defined VZ-like structures with packed SOX2$^+$ NPCs near the lumen at all three time points (Figures 3A–3C). At day 28, a layer containing a mixture of TBR2$^+$ IPCs and CTIP2$^+$ neurons formed above the VZ, reminiscent of the preplate (PP) in human cortical development (Figure 3A). By day 56, distinct SVZ-like structures containing a mixture of SOX2$^+$ NPCs, TBR2$^+$ IPCs, and immature neurons formed

above VZ, whereas cortical plate-like (CP) structures containing pure CTIP2$^+$ neurons formed above VZ and SVZ (Figure 3B).

One hallmark of embryonic human cerebral cortex is the prominence of specialized oRGCs in the oSVZ layer (Lui et al., 2011). Similar to the developing human cortex, a thin gap appeared to separate the expanded SVZ in day 84 organoids into an inner SVZ-like (iSVZ) region that contained densely packed TBR2$^+$ IPCs and an oSVZ-like region (Figure 3C). Recent studies have identified markers preferentially expressed by oRGCs in the developing human cortex, including HOPX, FAM107A, and PTPRZ1 (Pollen et al., 2015; Thomsen et al., 2015). Using antibodies that we validated with gestational week 22 (GW22) human tissue (Figure S3A), we found a large number of SOX2$^+$ HOPX$^+$ oRGCs in day 84 organoids (Figure 3D). Previous cerebral organoid protocols generated only sparse NPCs with apparent oRGC characteristics, which did not organize into a progenitor layer outside of VZ. In contrast, our forebrain organoids exhibited a distinct SOX2$^+$HOPX$^+$ oSVZ-like layer separated from the SOX2$^+$HOPX$^-$ VZ layer (Figure 3D). We sometimes observed HOPX$^+$ radially oriented basal processes from these oRGCs with pial contact but lacking an apical process (Figure S3B), a hallmark of human oRGCs (Hansen et al., 2010) (Figure S3A). Two other oRGC markers, FAM107A and PTPRZ1, were also specifically expressed in oSVZ (Figures 3E and 3G). Many oSVZ SOX2$^+$ progenitors were Ki67$^+$, indicating active cell division in this region (Figure 3F).

The presence of a prominent oRGC-like population in day 84 forebrain organoids offers an opportunity to track the time course of oRGC marker expression during organoid development. A recent study showed that oSVZ-exclusive expression of HOPX, FAM107A, and PTPRZ1 does not occur in the developing human cortex until gestational weeks 15–20 (Pollen et al., 2015). Interestingly, very limited HOPX expression was detected in day 28 organoids, while at day 56 its expression was prominent in both VZ and SVZ, but not exclusive to SVZ (Figure S3C).

Together, these results demonstrate that forebrain organoids exhibit multi-layer progenitor zone organization that recapitulates human cortical development, including a prominent oSVZ layer with oRGC-exclusive expression of defined molecular markers. Our system provides a platform to investigate the origin, properties, and mechanisms that define and regulate human oRGCs.

**Figure 2. Homogeneity of Early Stage Forebrain Organoids and Effects of BPA**

(A) Sample images and quantification among multiple iPSC cell lines and clones for immunostaining of organoids at day 14. Sample images for the "intrinsic protocol" are tiling multiple images over a large area. Scale bars, 100 μm. Values represent mean ± SEM (42–128 and 11–30 total neural tube structures from at least ten organoids each for the forebrain protocol and "intrinsic protocol," respectively; ***p < 0.005, Student's t test).

(B) Schematic drawing for SOX2$^+$ ventricular zone (VZ) and TUJ1$^+$ neuronal layer measurement in cortical structures (top) and box plot for relative VZ thickness in day 14 organoids. For each cortical structure, three measurements were taken at 45 degree angles to obtain the mean value. Relative VZ thickness is the ratio of VZ thickness to total thickness from ventricular surface to pial surface. The red dot indicates mean; upper and lower error bars in each box plot represent the top whisker (maximum value) and bottom whisker (minimum value), respectively (n = 30 and 15 cortical structures from at least ten organoids each for the forebrain and "intrinsic protocol," respectively).

(C and D) Sample images of immunostaining of organoids at day 28 (C; scale bars, 100 μm) and box plot for relative VZ thickness (D). Similar to (B) (n = 20 cortical structures from at least ten organoids each).

(E and F) Effect of BPA treatment of forebrain organoids from day 14 to 28. Shown are sample images of immunostaining of control and BPA-treated forebrain organoids (E) and quantification of relative VZ thickness (F) at day 28. Scale bar, 100 μm. Values represent mean ± SEM (n = 21 cortical structures from at least ten organoids; ***p < 0.0005, Student's t test).

Also see Figure S2.

(legend on next page)

Cell
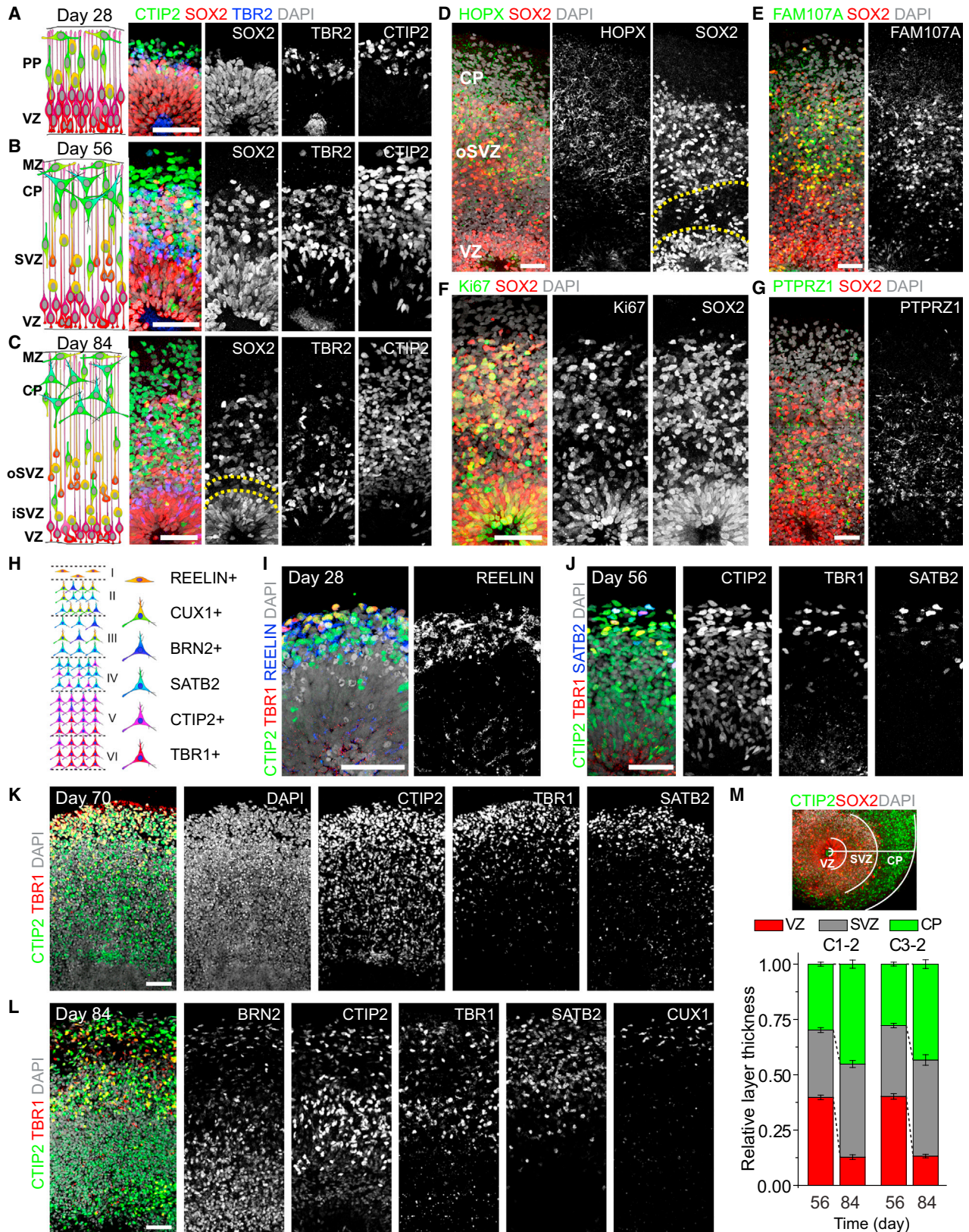
Generation of Diverse Neuronal Subtypes of All Six Cortical Layers

Next, we performed detailed expression analyses of markers for different neuronal subtypes (Figure 3H). At day 28, we observed neurons expressing deep-layer cortical neuron markers CTIP2 and TBR1, as well as neurons expressing the Cajal-Retzius cell marker REELIN (Figure 3I). At days 56 and 70, the SVZ contained neurons expressing a low amount of CTIP2, a feature of migrating immature neurons found in this region (Lui et al., 2011) (Figures 3J and 3K). The CP-like structure hosted a dense population of neurons expressing CTIP2 and TBR1, as well as a sparser population of neurons expressing upper-layer cortical neuron marker SATB2, which were localized close to the pial surface (Figures 3J and 3K). There was also a cell-sparse layer visualized by REELIN and DCX expression at the pial surface, resembling the marginal zone (MZ) that typically becomes layer I in vivo (Figure S3D). At day 84, late-born SATB2$^+$ neurons formed a layer partially separated from the early-born CTIP2$^+$ layer, suggesting specification of upper and deep cortical layers (Figure 3L). Furthermore, neurons expressing layer II/III markers CUX1 and BRN2 started to appear near the pial surface (Figure 3L). Quantification revealed CP and SVZ layer expansion and VZ layer reduction from days 56 to 84 (Figure 3M), resembling the developing human cortex.

Together, these results reveal the developmental time course of marker expression for neurons of all six cortical layers in forebrain organoids. Quantitative analysis of different organoids and human iPSC lines shows little variability in the relative thickness of different layers (Figure 3M), again indicating the robustness and reproducibility of our organoid system.

Molecular Signatures of Developing Forebrain Organoids

To further compare forebrain organoids to in vivo human brain development, we performed RNA-seq analyses of global transcriptomes from day 26, 40, 54, and 100 organoids. We compared organoid transcriptional profiles to datasets of 21 different human fetal organs during the first and second trimester (Roost et al., 2015). Pearson's correlation analysis showed that organoids from all four time points strongly correlated with fetal brains and spinal cord, with less or no correlation with other fetal somatic tissues (Figures 4A and S4A). Further comparison with transcriptomes from human dorsolateral prefrontal cortex samples across six life stages, ranging from fetal development to aged human tissue (Jaffe et al., 2015), showed the highest correlation with fetal brain tissues, with the best correlation for day 100 organoids (Figure S4B). Collectively, these results suggest that organoid development is reminiscent of fetal human brain development at the molecular level.

To pinpoint developmental stages and brain subregion identities of forebrain organoids, we performed large-scale comparisons with transcriptome datasets of 16 different human brain regions at 11 developmental stages (Figure S4C). These analyses revealed a temporal correlation between organoid and fetal human brain development, particularly for prefrontal cortex development (Figure 4B). For example, day 26–54 organoid profiles were closely related to several subregions of prefrontal cortex at 8–9 PCW (post-conception week), whereas day 100 organoids were more closely related to 17–24 PCW, or even 35 PCW for some subregions (Figures 4B and S4C).

We also identified differentially expressed genes during organoid development (Table S2). These genes also displayed similar trends over the course of in vivo brain development (Figures 4C and S4D). Gene ontology analysis revealed enrichment of many neuronal function pathways among upregulated genes (Figure 4D) and enrichment of cell-cycle-related pathways among downregulated genes (Figure S4E). Interestingly, differentially expressed genes during organoid development and risk genes for schizophrenia or autistic spectrum disorders showed significant overlap (p < 0.001, chi-square test; Figure 4E). Therefore, the organoid system can be used to study the functional impact of dynamic expression of these disease risk genes in human brain development.

Together, our systematic and comprehensive transcriptome comparisons provide additional validation that forebrain organoids resemble normal human embryonic cortical development.

Functionally Connected Cortical Neurons and GABAergic Neuronal Subtypes

To assess physiological properties of cells in organoids, we performed electrophysiological whole-cell recording in slices acutely sectioned from organoids. Recorded neurons were

---

Figure 3. Organization and Marker Expression of Different Progenitor Zones and Cortical Neuron Subtypes

(A–C) Schematic representations and sample immunostaining images of forebrain organoids at days 28 (A), 56 (B), and 84 (C). Scale bars, 50 μm. Dashed lines highlight a gap between oSVZ and iSVZ (C). PP, preplate; VZ, ventricular zone; MZ, marginal zone; CP, cortical plate; SVZ, subventricular zone; oSVZ, outer subventricular zone; iSVZ, inner subventricular zone.

(D–G) Sample images of immunostaining of oRGC markers HOPX (D, tiling image), FAM107A (E), PTPRZ1 (G), and Ki67 (F) in day 84 forebrain organoids. Scale bars, 50 μm.

(H) Schematic representation of marker expression for cortical neurons in the mature mammalian neocortex.

(I) Sample images of immunostaining for preplate Cajal-Retzius cell marker REELIN and deep-layer neuron markers CTIP2 and TBR1 in day 28 forebrain organoids. Scale bar, 50 μm.

(J and K) Sample images of immunostaining for CTIP2, TBR1, and superficial layer neuron marker (SATB2) in forebrain organoids at days 56 (J) and 70 (K). Images shown in (K) are from consecutive sections for the same cortical structure. Scale bars, 50 μm.

(L) Sample images of immunostaining for CTIP2, TBR1, and superficial layer neuron markers (SATB2, BRN2 and CUX1) in forebrain organoids at day 84. Images shown are from consecutive sections for the same cortical structure. Scale bar, 50 μm.

(M) Sample image showing layer specification in forebrain organoids and quantification of the relative thickness of VZ, SVZ, and CP at days 56 and 84 for two iPSC lines. For each cortical structure, three measurements were taken at 45 degree angles to obtain the mean. Values represent mean ± SEM (n ≥ 6 cortical structures from six organoids).
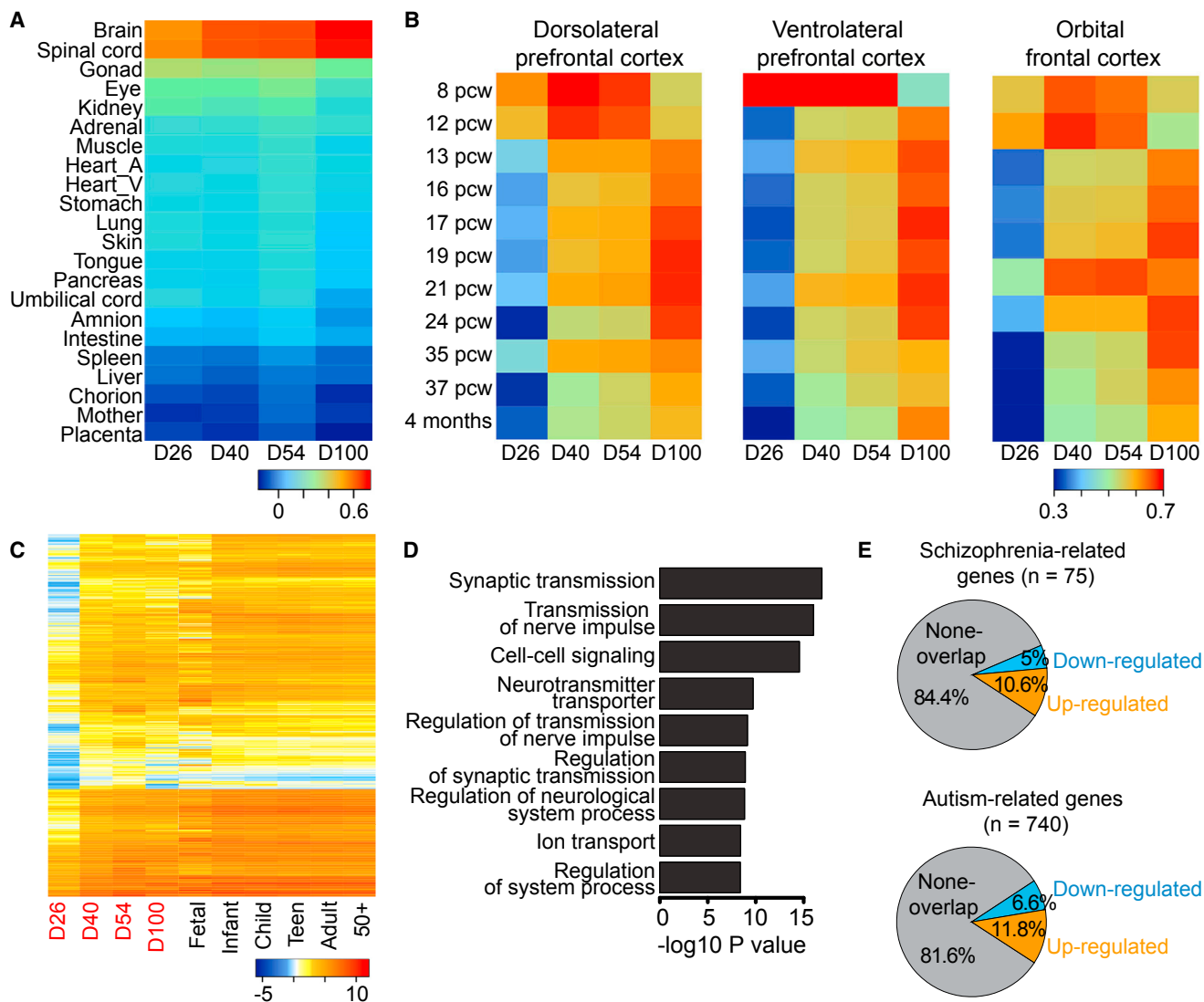
Also see Figure S3.

Cell

Figure 4. Correlation of Global Transcriptomes between Forebrain Organoids and Fetal Human Brain Development

(A) Heatmap of Pearson's correlation analysis of RNA-seq datasets from day 26, 40, 54, and 100 organoids and published datasets from 21 different human fetal organs (Roost et al., 2015). Shown are averaged values for biological replicates.

(B) Heatmaps of Pearson's correlation analysis of RNA-seq datasets among forebrain organoids at different stages and published transcriptome datasets of 3 different cortical subregions at 11 developmental stages from Allen Brain Atlas. See Figure S5C for comparison of all 16 different human brain regions.

(C) Heatmap of gene expression dynamics from upregulated genes between day 26 and later stages of organoid development.

(D) Gene ontology analysis of upregulated genes. Nine top terms (in terms of p values) are shown.

(E) Overlap of differentially expressed genes during organoid development with known schizophrenia-related risk genes (from http://bioinfo.mc.vanderbilt.edu/SZGR/) and autism-related risk genes (from https://gene.sfari.org/autdb/HG_Home.do). Overlapping genes are statistically significant (p < 0.001, chi-square test). Also see Figure S4 and Table S2.

capable of firing trains of TTX-sensitive action potentials (Figures 5A and S5A). Neurons showed rectifying membrane properties, Na^+ and K^+ currents in response to voltage ramps (Figure S5B). Cells with linear membrane properties were also observed, indicating presence of astrocytes (Figure 5B). We observed developmental changes of intrinsic properties in recorded neurons across different stages (Figures S5C–S5I).

To visualize morphology of individual neurons, we electroporated organoids to sparsely label cells with GFP. At day

85, GFP^+ neurons exhibited complex neuronal morphology with spine-like structures in close association with presynaptic $SV2^+$ puncta (Figure 5C). About 50% of cells recorded showed spontaneous excitatory postsynaptic current (sEPSC) that was sensitive to the glutamate receptor antagonist DNQX (Figure 5D). Both intrinsic properties and synaptic connectivity were similar between two iPSC clones (Figures S5J and S5K).

One hallmark of neuronal maturation is the switch from a depolarizing response to GABA to hyperpolarizing due to

developmentally regulated changes in intracellular Cl⁻ concentration, mediated by NKCC1 downregulation and KCC2 upregulation (Ben-Ari and Spitzer, 2004). We found that NKCC1 was expressed at both days 56 and 84, whereas KCC2 was strongly expressed in the CP at day 84 but minimally at day 56 (Figure S5L). We further performed a functional assay to monitor Ca^{2+} rise in response to GABA-induced depolarization (Figure 5E). Quantification showed an increase over time in the percentage of neurons without GABA-induced Ca^{2+} rise among all neurons that responded to glutamate (Figure 5F). Therefore, forebrain organoids exhibit functional features of neuronal maturation found in vivo.

We also found $GABA^+VGLUT1^-$ neurons in forebrain organoids after day 84 (Figure 5G). Electrophysiological recordings in the presence of DNQX to block all glutamatergic synaptic transmission also showed spontaneous postsynaptic currents with slower kinetics (Figure 5H). Immunohistological analysis further revealed the presence of at least three major subtypes of GABAergic neurons expressing parvalbumin, nNOS, or somatostatin (Figure 5I). Consistent with electrophysiological recording results (Figure 5B), we observed $S100\beta^+$ and $GFAP^+$ astrocytes in close association with surrounding neurons (Figures 5J and 5K). Together, these findings demonstrate that forebrain organoids contain a diverse collection of neuronal and other cell types found in developing human brains.

Generation of Midbrain and Hypothalamic Organoids

We next explored approaches to generate organoids with other brain region identities. Building upon a 2D differentiation protocol for generating midbrain dopaminergic (DA) neurons (Kriks et al., 2011), we applied Sonic hedgehog (SHH) agonists (recombinant SHH and Purmorphamine), FGF-8, SMAD inhibitors (SB431542 and LDN193189), and GSK3β inhibitor (CHIR99021) to induce floor-plate differentiation of human iPSCs, which were transferred to SpinΩ at day 14 (Figure 6A). At day 18, midbrain organoids showed organized neuroepithelium-like structures expressing NESTIN and floor-plate precursor marker FOXA2, but not DA neuron marker TH, whereas very few cells expressed forebrain marker PAX6 or hypothalamus progenitor marker RAX1 (Figures 6B and S6A). At day 38, we observed numerous TH^+ DA neurons (Figure 6C). At day 56, the majority of TH^+ neurons expressed $FOXA2^+$ and dopamine transporter (DAT) (Figure S6B). In addition, midbrain organoids contained TH^+ cells that expressed midbrain DA neuron markers NURR1 and PITX3 (Figure S6B). At day 75, PITX3 was robustly expressed by TH^+ cells, suggesting specification of A9 DA neurons (Chung et al., 2005) (Figure 6D). To quantify TH and FOXA2 expression, we dissociated midbrain organoids at day 65. Upon culturing in monolayer for 5 days, we found that 95% ± 1% of cells were $FOXA2^+$ and 55% ± 4% were TH^+ DA neurons (n = 6; Figure 6E).

We also explored methods to generate hypothalamic organoids from human iPSCs. We first treated human iPSCs with dual SMAD inhibitors (SB431542 and LDN193189) to pre-pattern them to the neuroectodermal fate (Figure 6F). After 3 days, embryoid bodies were treated with WNT3A, SHH, and Purmorphamine to induce the hypothalamic lineage. At day 8, the majority of cells in organoids expressed NKX2.1, NKX2.2,

RAX1, SOX2, NESTIN, and FOXA2, markers that are consistently expressed during early hypothalamus development (Blackshaw et al., 2010) (Figure 6G). At day 40, peptidergic neuronal markers, including POMC, VIP, OXT, and NPY, were detected in organoids generated from different iPSC lines (Figure 6H). At day 40, but not day 8, a subset of cell populations expressed OTP, a homeobox protein essential for specification of hypothalamic neuronal lineages (Wang and Lufkin, 2000) (Figures 6H and S6C). Together, these findings demonstrate the versatility of SpinΩ to support growth of organoids of different types.

Modeling ZIKV Exposure during Cortical Neurogenesis

Our organoid system provides a quantitative platform to model human diseases. The World Health Organization recently declared ZIKV a Public Health Emergency of International Concern, due in part to the uncertainty surrounding increased reports of microcephaly and other neurological disorders coinciding with clusters of ZIKV outbreaks (Heymann et al., 2016). Recent studies of human NPCs in 2D and neurosphere cultures showed efficient infection by ZIKV, leading to increased cell death and attenuated growth (Tang et al., 2016; Garcez et al., 2016). Without organizational features unique to 3D brains, such as cortical layers, these initial studies in 2D cultures do not directly address the potential link between ZIKV and microcephaly. It also remains unknown whether ZIKV exhibits specific tropism for different neural cell types in more complex 3D tissue.

We performed a series of experiments to model transient ZIKV exposure at different stages of human cortical development by incubating forebrain organoids with ZIKV in medium for 24 hr in SpinΩ. We initially used a prototype ZIKV strain of African lineage (MR766, termed $ZIKV^M$ hereafter) (Haddow et al., 2012). $ZIKV^M$ readily infected $SOX2^+$ NPCs in day 14 forebrain organoids (Figures 7A and S7A). After 18 days, $ZIKV^M$ infection resulted in overall decreased organoid size (Figures S7B and S7C). Quantitative analyses showed dramatically reduced VZ thickness and size (Figures S7D and S7E), likely due to significant cell death and suppression of NPC proliferation (Figures 7B and 7C). We also observed a significant increase in lumen size within ventricular structures (Figure S7F), reminiscent of dilated ventricles in a recently reported clinical case of a fetal brain infected with ZIKV (Driggers et al., 2016).

Next, we exposed day 28 organoids that contained both progenitor and neuronal layers to two different doses of $ZIKV^M$ (1× and 0.25×; Figure S7G). Most $ZIKV^M$-infected cells were $SOX2^+$ NPCs, and very few were $TBR2^+$ IPCs or $CTIP2^+$ immature neurons when quantified 4 days later (Figure 7D), suggesting specific tropism of $ZIKV^M$ toward NPCs in the 3D tissue. After 14 days, we observed a significantly increased number of $ZIKV^M$-infected cells (Figure S7H), consistent with productive infection by ZIKV. In addition to overall size reduction (Figure S7I), we observed a ZIKV dose-dependent decrease of EdU^+-proliferating cells and increased $CAS3^+$ cells (Figures 7E and S7J). Interestingly, many $CAS3^+$ cells were $ZIKV^-$, indicating a non-cell-autonomous effect (Figure S7J). As a result, ZIKV infection of early stage organoids, corresponding to the first trimester of human fetal development, led to a significant reduction in both VZ and neuronal layer thickness (Figure 7F), resembling microcephaly.
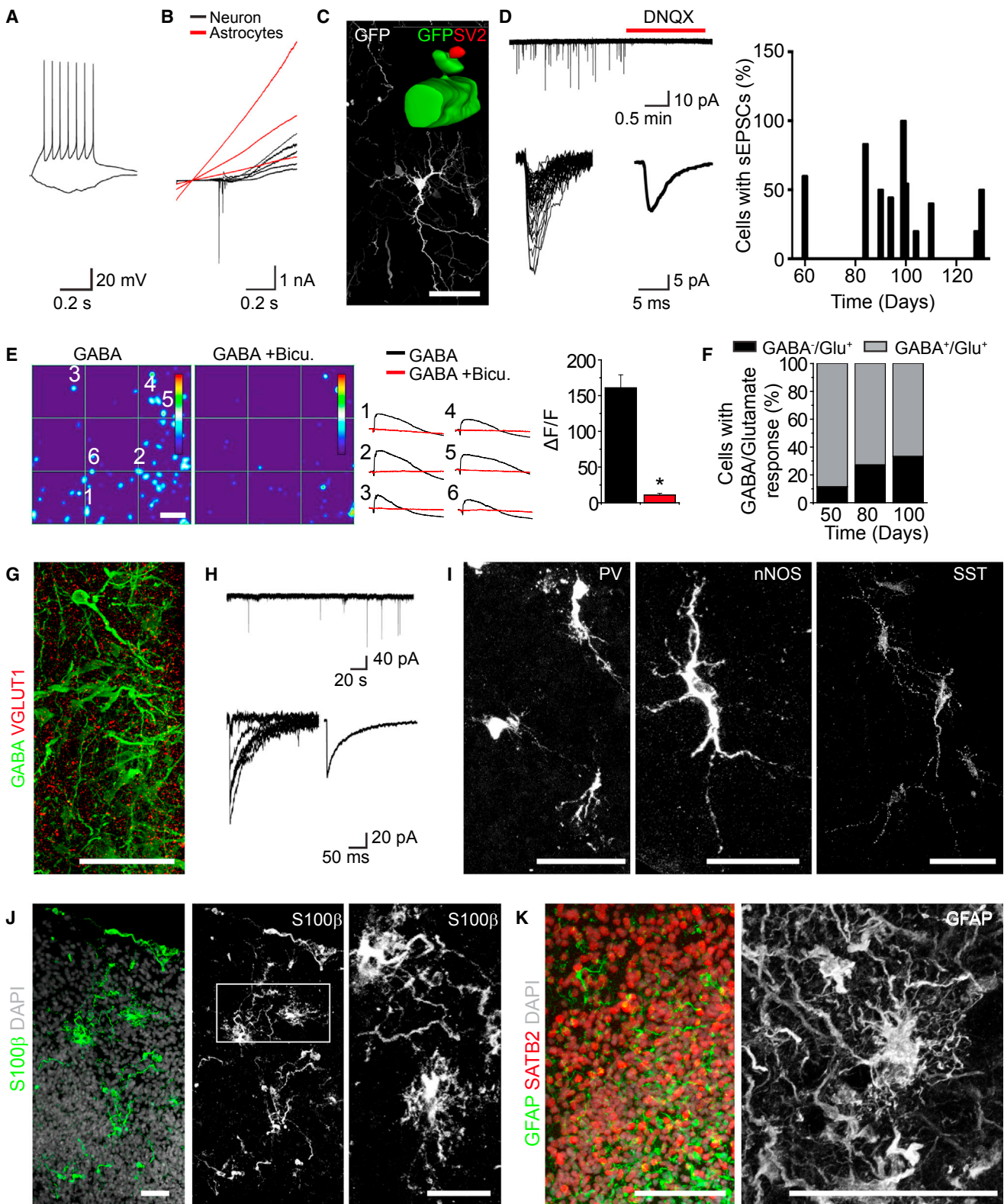
Cell

Figure 5. Functional Characterization of Forebrain Organoids

(A–D) Electrophysiological and morphological analyses of cells in forebrain organoids. Shown in (A) are sample current-clamp traces of a neuron firing a train of action potentials in response to 10 pA current injection. A hyperpolarizing step of −5 pA is also shown. Shown in (B) are sample voltage-clamp traces showing

(legend continued on next page)

We also assessed the effect of ZIKV^M on day 80 forebrain organoids (Figure S7K). After 10 days, we again observed preferential localization of ZIKV^M in SOX2$^+$ NPCs in VZ and oSVZ, but it was also detected in CTIP2$^+$ neurons and occasionally in GFAP$^+$ astrocytes (Figures 7G and 7H). The infection appeared less robust compared to that of earlier stages of organoids, possibly due to limited ZIKV penetration to the interior of organoids where NPCs reside. After 20 days, we observed an increased number of ZIKV$^+$ cells (Figure 7I). Quantification showed a higher percentage of SOX2$^+$ NPCs with ZIKV^M than that for CTIP2$^+$ neurons (Figure 7I). The presence of ZIKV$^+$SOX2$^+$HOPX$^+$ cells indicates infection of oRGCs by ZIKV (Figure 7J).

Two recent studies have shown few differences between properties of different ZIKV strains in different models (Bayer et al., 2016; Lazear et al., 2016). We explored a ZIKV strain of Asian lineage that exhibits >99% amino acid sequence similarity to strains currently circulating in Brazil (FSS13025, termed ZIKV^C hereafter) (Haddow et al., 2012). Quantitative analysis showed similar enrichment of ZIKV^C in SOX2$^+$ NPCs, compared to CTIP2$^+$ immature neurons or TBR2$^+$ IPCs in early stage organoids (Figures S7L and S7M).

Together, our forebrain organoid system allowed quantitative investigation of consequences of ZIKV exposure, and our results suggest that ZIKV, upon access to the fetal brain, targets NPCs and causes microcephalic-like deficits in cortical development.

DISCUSSION

We have developed a cost-effective, simple-to-use system for 3D organoid cultures by designing a miniaturized multi-well spinning bioreactor, SpinΩ, which can be used with standard cell-culture plates. The low cost of the platform allowed us to optimize protocols to generate forebrain organoids with minimized heterogeneity and variability that enables quantitative analyses and better recapitulation of the developing human cortex. Specifically, these forebrain organoids exhibit a well-developed oSVZ-like region containing NPCs that share molecular and morphological features of human oRGCs, organized neuronal subtypes found in all six cortical layers, and GABAergic neuronal subtypes. We further demonstrated SpinΩ's versatility by developing protocols to generate organoids recapitulating character-istics of other brain regions. Finally, we applied our forebrain organoid platform for chemical compound testing and modeling ZIKV infection.

SpinΩ, a Miniaturized Spinning Bioreactor for Cost-Effective Organoid Culturing

Several pioneering studies showed that cerebral organoid systems offer improved growth conditions for 3D tissue, leading to a more representative model of the developing human brain (Danjo et al., 2011; Kadoshima et al., 2013; Lancaster et al., 2013; Mariani et al., 2015; Paşca et al., 2015). In particular, the use of a spinning flask provides a 3D low-shear stress suspension culture with enhanced diffusion of oxygen and nutrients that supports formation of larger, continuous cortical structures (Lancaster et al., 2013). Under our culture conditions, direct comparison with stationary and orbital shaker cultures confirmed the beneficial effect of spinning for forebrain organoids. However, maintaining organoids in standard spinning flasks makes it cost prohibitive to supplement the media with small molecules and growth factors to promote growth and differentiation of organoids. Our miniaturized spinning bioreactor SpinΩ addresses this limitation by dramatically reducing the required media volume, allowing for systematic and efficient testing of culture conditions in parallel. Moreover, SpinΩ's small footprint and compact shape reduces the incubator space required, a feature that is further highlighted by the stackable version (Figure S1A). Many of the design parameters of SpinΩ, including number and size of wells, rotation speed, shaft angle, and shape, can be customized based on specific needs. Together, the SpinΩ system provides better accessibility and higher efficiency for developing 3D tissue cultures for applications related to the brain and other organs.

Features of Forebrain Organoids and Areas for Improvements

Compared to several pioneering cerebral organoid systems, our forebrain organoids show high reproducibility, which is critical to realize its promise as a standardized model for human cortical development. Two rounds of patterning factors effectively induce forebrain differentiation and significantly reduce both tissue and temporal development heterogeneity. Our proof-of-principle study with BPA, although with concentrations likely

currents in response to a ramp protocol (−90 to 110 mV). Shown in (C) is a sample tiling image of a neuron in a day 85 forebrain organoid labeled by GFP upon electroporation. The insert shows surface rendering of a dendritic spine structure on a GFP$^+$ neuron with the pre-synaptic terminal labeled by SV2 staining in red. Scale bars, 50 μm. Shown in (D, left) are sample recording traces of sEPSCs and pharmacological blockade by DNQX. Identified sEPSC events are overlaid, and the average sEPSC trace is shown. Also shown in (D, right) is the summary of the percentage of cells that exhibited detectable sEPSC events in organoids of different ages.

(E) Calcium imaging analysis of cellular response to GABA application (10 μM). Day 100 organoids were loaded with Fluo-4. Shown in left panels are sample heatmaps of GABA-induced fluorescence changes (ΔF/F) within the same region in the absence or presence of Bicuculline (Bicu. 50 μM). The color scale at the right indicates a ΔF/F range of 0% to 250%. Scale bar, 50 μm. Shown in the middle panel are calcium response curves for individual cells indicated in the heatmap. Shown in the right panel is the summary of ΔF/F in response to GABA in absence or presence of bicuculline. Values represent mean ± SEM (n = 43 neurons from three organoids).

(F) Developmental shift of the percentage of cells in forebrain organoids that exhibit calcium rise in response to GABA (10 μM) and glutamate (20 μM). Value represents mean (n = 26, 77, and 69 neurons from three organoids at days 50, 80, and 100, respectively).

(G–I) GABAergic neurons in forebrain organoids. Shown are sample images of immunostaining for GABA and VGLUT1 (G) and GABAergic neuron subtypes (I). Scale bars, 50 μm. Shown in (H) are sample recording traces of sIPSCs. Identified sIPSC events are overlaid, and the average sIPSC trace is shown.

(J–K) Sample images of immunostaining for astrocyte markers S100β (J) and GFAP (K) in organoids over 100 days. Scale bars, 50 μm.
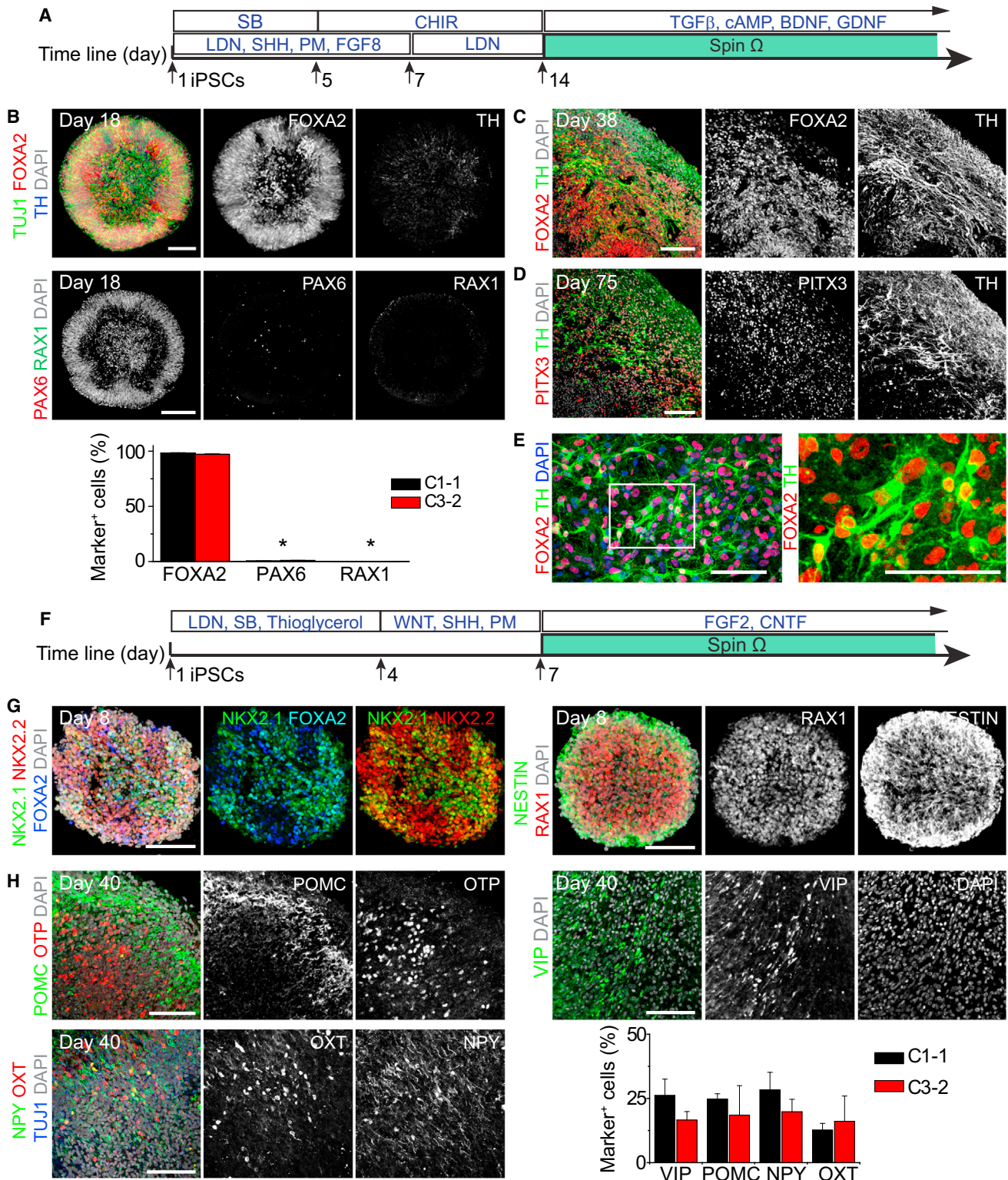
Also see Figure S5.

Figure 6. Generation of Midbrain and Hypothalamic Organoids

(A–E) Midbrain organoids from human iPSCs. Shown in (A) is a schematic diagram of the midbrain organoid protocol. Shown in (B) are sample images of day 18 organoids (scale bars, 100 μm) and quantifications. Values represent mean ± SEM (n = 4 organoids each; *p < 0.05, Student's t test). Also shown are sample

(legend continued on next page)

higher than normal human exposure, demonstrates that many parameters in these organoids can be reliably quantified; therefore, this platform can be broadly used for drug testing, compound screening, and disease modeling.

Forebrain organoids better recapitulate developing human cortex along multiple dimensions, as compared to previously reported methods. First, these forebrain organoids contain a well-defined oSVZ-like region with a prominent oRGC-like NPC layer, which are distinct features of developing human cortex that are absent in rodents and previous organoid models. Time course of SVZ and oSVZ layer formation and progression also models dynamic changes during human cortical development. Moreover, oRGCs in forebrain organoids express three recently identified human oRGC markers. Second, forebrain organoids robustly generate organized cortical neurons expressing markers found in all six layers of human cortex, including a layer of CUX1^{+} neurons destined for layer II. The peak in production of late-born neurons expressing the upper-layer neuron marker SATB2 occurred after day 56, coinciding with oSVZ specification and expansion. Because the peak of oSVZ proliferation coincides in time with formation of upper cortical layers, which are particularly cell dense in human cortex, it has been suggested that the abundant oRGC population in human oSVZ is responsible for this evolutionary distinction (Lui et al., 2011). Therefore, the presence of well-developed oSVZ may be responsible for robust generation of upper-layer neurons in forebrain organoids. Our electrophysiology and calcium imaging analyses revealed functional neuronal properties, active synaptic transmission, and recapitulation of neuronal maturation characteristics similar to those observed in vivo. We show the presence of GABAergic neuronal subtypes in organoids. The apparent absence of NKX2.1[+] ventral progenitors during early differentiation suggests a possible dorsal origin of GABAergic neurons, a distinct feature of primates and humans (Petanjek et al., 2009; Yu and Zecevic, 2011). Lastly, large-scale comparisons of global transcriptome analyses confirm that forebrain organoid development closely correlates with human cortical development at the molecular level. Forebrain organoids with a well-developed oSVZ will significantly expand our ability to study distinct characteristics of human cortical development that cannot be represented in rodent models. Compared to studies of postmortem human tissues, forebrain organoids offer a model to investigate embryonic human cortical development as a continuous dynamic process in live cells and allow pharmacological and genetic manipulations to investigate underlying mechanisms.

It is likely that continued optimization can further improve the forebrain organoid system. First, depletion of nutrients and oxygen in the interior of organoids is one factor limiting our ability to model human brain development beyond the second trimester. Due to dramatic CP expansion, progenitor zones in forebrain organoids become gradually depleted after day 100. One potential solution is to engineer vascularized 3D tissue by endothelial cell co-cultures or by implementing microfluidic perfusion networks. An alternative approach would be to explore culture conditions that can accelerate forebrain organoid development to produce features of late-stage cortical development with smaller overall organoid size. Second, forebrain organoids do not contain well-defined regions representing the intermediate zone (IZ) and subplate, which play important roles in neuronal migration during cortical development. Intriguingly, a previously reported cortical neuroepithelial system showed formation of a cell-sparse IZ-like region despite lacking oSVZ (Kadoshima et al., 2013). Third, although we have identified cortical neurons expressing markers found in all six human cortical layers, they display only rudimentary separation. Additional chemical and physical cues may be required to better regulate neuronal migration and positioning.

Modeling ZIKV Exposure during Different Stages of Cortical Neurogenesis

As an application of our organoid platform for disease modeling, we modeled the impact of ZIKV exposure at different stages of pregnancy. Recent clinical studies have established that ZIKV can pass through placenta to gain access to the developing fetal brain (Calvet et al., 2016; Driggers et al., 2016; Mlakar et al., 2016). We show that, among different cell types in 3D tissue, ZIKV exhibits specific tropism toward NPCs, including oRGCs, although ZIKV could be detected in immature neurons, IPCs, and astrocytes. Time-course analysis further shows that ZIKV infection in NPCs is productive, resulting in more infected cells over time. Therefore, even a very low-dose and transient ZIKV exposure in utero may have a prolonged and increasingly severe effect over time. Consistent with clinical findings that first trimester infections are the most dangerous (Cauchemez et al., 2016; Faria et al., 2016), exposure of early stage forebrain organoids to ZIKV for only 1 day leads to detrimental effects, mimicking many features of microcephaly, including decreased neuronal layer thickness and overall size as well as enlarged lumen/ventricles. Mechanistically, we show increased cell death and suppressed proliferation of infected NPCs. The same ZIKV treatment of day 80 organoids, which are more complex and resemble the second trimester, also leads to preferential infection of SOX2^{+} NPCs, including HOPX[+] oRGCs. Together, our results provide compelling evidence that, upon access to the fetal brain, productive and preferential infection of NPCs by ZIKV leads to characteristic features resembling microcephaly. Forebrain organoids therefore provide a quantitative experimental platform for future studies to investigate the impact of ZIKVs, identify cellular and molecular mechanisms, and screen for therapeutic interventions, issues that are critical to resolving the current global health emergency related to ZIKV.

---

images of immunostaining of midbrain organoids at days 38 (C) and 75 (D) and monolayer cultures 5 days after dissociation and plating of day 65 midbrain organoids (E). Scale bars, 50 μm.

(F–H) Hypothalamic organoids. Shown in (F) is a schematic diagram of the hypothalamic organoid protocol. Shown are sample images of day 8 (G) and day 40 (H) organoids. Scale bars, 100 μm. Also shown in (H) is a summary of quantification for peptidergic neuronal marker expression in day 40 hypothalamic organoids from two iPSC lines. Values represent mean ± SEM (n = 3 organoids each).

Also see Figure S6.
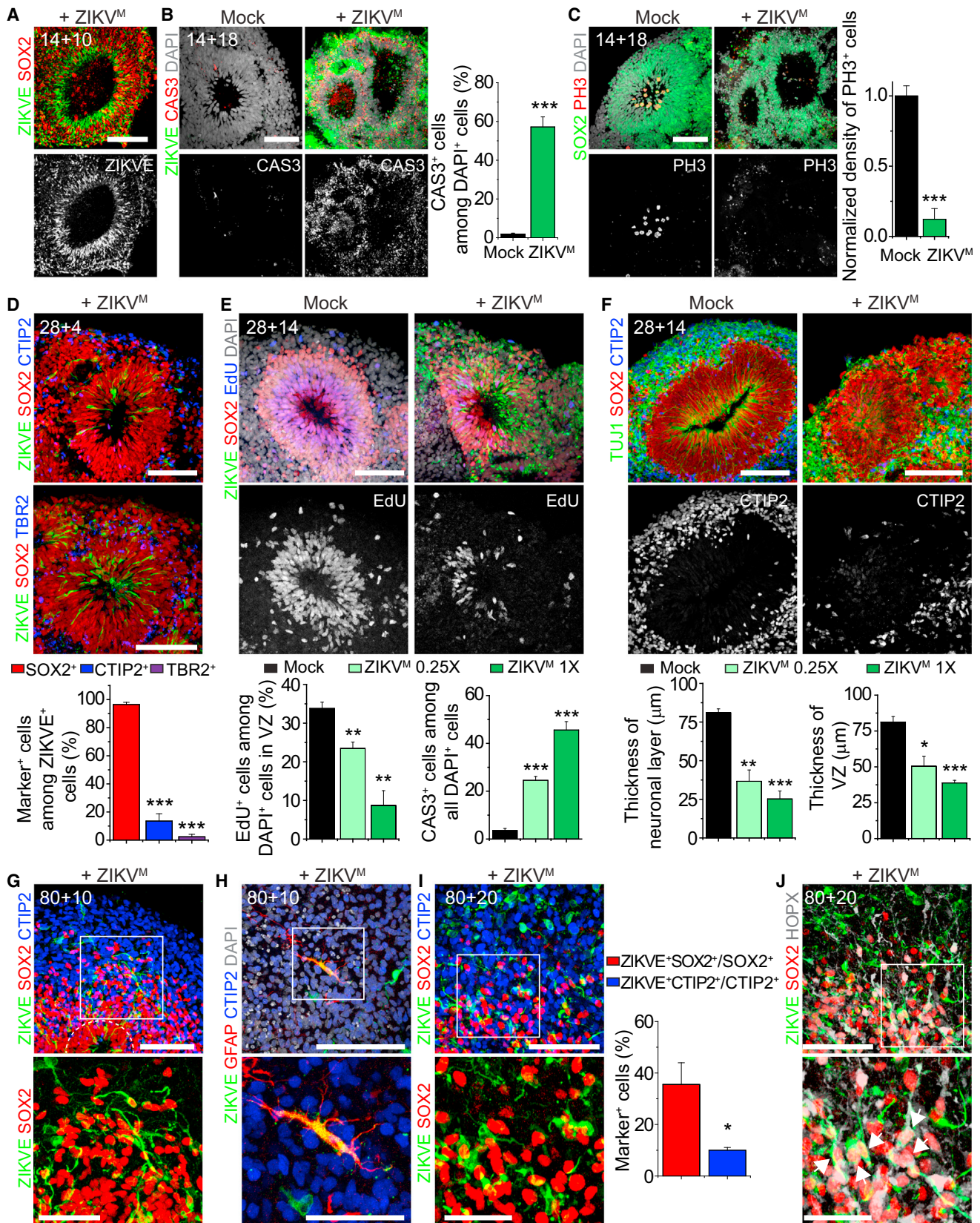
(legend on next page)

Additional Future Applications

Brain organoids also provide a renewable source of human neurons and other cell types, such as DA neurons for transplantation in models of Parkinson's disease. Organoid growth is coupled with dramatic expansion in cell numbers. For example, embryoid bodies of around 300 μm in diameter could expand to organoids that are up to 3 mm in diameter, achieving a 1,000-fold expansion in cell mass. Just as the cerebral organoid methodology was inspired by self-organizing tissue organoids developed for other organs, SpinΩ has the potential to be broadly applied to other types of 3D tissue cultures beyond the nervous system, where SpinΩ's advantages in reduced cost, increased throughput, enhanced cell survival, and improved factor absorption would prove beneficial. The modular stackable version of SpinΩ allows for consistent culture conditions for multiple plates simultaneously and potential large-scale 3D tissue cultures and drug screening.

EXPERIMENTAL PROCEDURES

Bioreactor Design and 3D Printing

We used SolidWorks for design and drawings of all components for 3D printing. Modular individual bioreactors were made to fit into a stackable bioreactor with some modifications. The blueprints for 3D printing of the 12-well version and the stackable version of the bioreactor are provided in Data S1. Each folder contains the CAD files for design of each component as well as a PDF reference file to view the full assembly of the pieces.

Culture of Brain-Region-Specific Organoids, Immunohistology, and Quantification

All studies were performed with approved protocols of Johns Hopkins University School of Medicine. Human iPSC lines were previously characterized (Wen et al., 2014). See detailed protocols to generate forebrain (Figure 1B), midbrain (Figure 7A), and hypothalamic organoids (Figure 7F) in the Supplemental Experimental Procedures.

Whole organoids were processed for immunocytochemistry, as previously described (Yoon et al., 2014). See the list of antibodies and their information in Table S1. For cell-fate quantifications of day 14 organoids, neural tube structures were counted as positive for forebrain markers when >80% of all nuclei were positive for respective markers. Markers for different brain regions were quantified by measuring the area stained positive for markers and normalized to DAPI in ImageJ software. VZ was defined by SOX2 immunoreactivity and neural-tube morphology, and the outer layer was defined by the area outside of the VZ to the nearest pial surface. The relative VZ thickness was defined as the ratio of VZ thickness to VZ plus outer layer thickness. Layer thickness measurements at days 56 and 84 in forebrain organoids were performed similarly with the addition of SVZ. SVZ was defined by the region within mixed populations of SOX2^{+} and CTIP2^{+} nuclei outside of VZ. CP was defined by the region from the boundary of SVZ to the pial surface with exclusive CTIP2^{+} nuclei. Some sample images shown were from tiling multiple images of a large area as indicated.

RNA-Seq and Bioinformatics Analyses

Forebrain organoids at days 26, 40, 54, and 100 were processed for RNA-seq and bioinformatics analyses, as previously described (Tang et al., 2016). Sequence read counts for 22 different human fetal organs were obtained from GSE66302. Human dorsolateral prefrontal cortex RNA-seq datasets from six different life stages were obtained from www.nature.com/neuro/journal/v18/n1/extref/nn.3898-S9.zip. RNA-seq gene expression for 11 time points of fetal development and 16 different brain regions were obtained from Allen Brain Atlas (www.brain-map.org). Schizophrenia-related risk genes were obtained from http://bioinfo.mc.vanderbilt.edu/SZGR. Autism-related risk genes were obtained from https://gene.sfari.org/autdb/HG_Home.do. R programming language was used to perform all data analysis and generate the figures.

Electrophysiology and Calcium Imaging

Organoid slices were prepared by embedding organoids in 4% low melting point agarose cooled to ∼32°C. Slices (250 μm) were sectioned and were immediately ready for recording. Calcium imaging was performed similarly, as previously described (Kim et al., 2012).

Modeling ZIKV Exposure

ZIKV was prepared and titered as previously described (Tang et al., 2016). Supernatant from ZIKV-infected mosquito C6/36 cells (ZIKV[M]) or Vero cells (ZIKV[C]) was diluted 1:10 (1×) or 1:40 (0.25×) and applied directly in SpinΩ for 24 hr and then replaced with fresh medium. Forebrain organoids infected at day 28 were pulsed with 10 μM EdU for 2 hr on day 42 and were fixed for analysis 24 hr later. Quantitative analyses were conducted on randomly picked cortical structures. Cell death was quantified by counting CAS3^{+} nuclei over total nuclei stained by DAPI. Area of VZ and lumen and thickness of VZ and neuronal layers were measured using ImageJ software. Overall size of organoids was measured under calibrated 4× bright field microscope.

ACCESSION NUMBERS

The accession number for RNA-seq data reported in this paper is GEO: GSE80073.

SUPPLEMENTAL INFORMATION

Supplemental information includes Supplemental Experimental Procedures, seven figures, two tables, and one data file and can be found with this article online at http://dx.doi.org/10.1016/j.cell.2016.04.032.

Figure 7. Modeling Impact of ZIKV Exposure Using Forebrain Organoids

(A) Sample immunostaining images of forebrain organoids exposed to ZIKV[M] (1×) or mock treated at day 14 for 24 hr and analyzed 10 days later (14+10). Scale bar, 100 μm. ZIKVE, Zika virus envelop protein.

(B and C) Sample immunostaining images of forebrain organoids exposed to ZIKV[M] (1×) or mock treated at day 14 for 24 hr and analyzed 18 days later (14+18) for CAS3 (B) or PH3 (C). Scale bars, 100 μm. Also shown are quantifications for the percentage of CAS3^{+} cells among the total number of nuclei stained by DAPI (B) and density of PH3^{+} cells within VZ (C). Values represent mean ± SEM (n = 5 organoids; ***p < 0.0005, Student's t test).

(D) Sample immunostaining image of a forebrain organoid exposed to ZIKV[M] (1×) at day 28 for 24 hr and analyzed 4 days later (28+4) (scale bars, 100 μm) and quantifications. Values represent mean ± SEM (n = 5 cortical structures from three organoids; ***p < 0.0005, Student's t test).

(E and F) Forebrain organoids exposed to ZIKV[M] (1× or 0.25×) or mock treated at day 28 for 24 hr and analyzed 14 days later (28+14). Shown are sample immunostaining images and quantification of cell proliferation and cell death in ZIKV-infected regions (E) and thickness of SOX2^{+} VZ layer and TUJ1^{+} neuronal layer (F). Scale bars, 100 μm. Values represent mean ± SEM (n = 5 cortical structures from three organoids; *p < 0.05; **p < 0.005, ***p < 0.0005, Student's t test).

(G–J) Sample immunostaining images (top; scale bars, 100 μm) and magnified views (bottom; scale bars, 50 μm) of forebrain organoid exposed to ZIKV[M] (1×) at day 80 for 24 hr and analyzed 10 (80+10; G and H) or 20 days later (80+20; I and J). Arrows in (J) point to ZIKV[+]HOPX[+]SOX2^{+} oRGC-like cells in the oSVZ region. Also shown in (I) are quantifications for the percentage of ZIKV^{+} cells among the total number of SOX2^{+} or CTIP2^{+} cells in the whole cortical structure. Values represent mean ± SEM (n = 7 cortical structures from five organoids; *p < 0.05, Student's t test).

Also see Figure S7.

Cell

REFERENCES

Bayer, A., Lennemann, N.J., Ouyang, Y., Bramley, J.C., Morosky, S., Marques, E.T.J., Cherry, S., Sadovsky, Y., and Coyne, C.B. (2016). Type III interferons produced by human placental trophoblasts confer protection against Zika virus infection. Cell Host Microbe. Published online April 5, 2016. http://dx.doi.org/10.1016/j.chom.2016.03.008.

Ben-Ari, Y., and Spitzer, N.C. (2004). Nature and nurture in brain development. Trends Neurosci. 27, 361.

Blackshaw, S., Scholpp, S., Placzek, M., Ingraham, H., Simerly, R., and Shimogori, T. (2010). Molecular pathways controlling development of thalamus and hypothalamus: from neural specification to circuit formation. J. Neurosci. 30, 14925–14930.

Calvet, G., Aguiar, R.S., Melo, A.S., Sampaio, S.A., de Filippis, I., Fabri, A., Araujo, E.S., de Sequeira, P.C., de Mendonça, M.C., de Oliveira, L., et al. (2016). Detection and sequencing of Zika virus from amniotic fluid of fetuses with microcephaly in Brazil: a case study. Lancet Infect. Dis. Published online February 17, 2016. http://dx.doi.org/10.1016/S1473-3099(16)00095-5.

Cauchemez, S., Besnard, M., Bompard, P., Dub, T., Guillemette-Artur, P., Eyrolle-Guignot, D., Salje, H., Van Kerkhove, M.D., Abadie, V., Garel, C., et al. (2016). Association between Zika virus and microcephaly in French Polynesia, 2013-15: a retrospective study. Lancet.

Chung, S., Hedlund, E., Hwang, M., Kim, D.W., Shin, B.S., Hwang, D.Y., Kang, U.J., Isacson, O., and Kim, K.S. (2005). The homeodomain transcription factor Pitx3 facilitates differentiation of mouse embryonic stem cells into AHD2-expressing dopaminergic neurons. Mol. Cell. Neurosci. 28, 241–252.

Danjo, T., Eiraku, M., Muguruma, K., Watanabe, K., Kawada, M., Yanagawa, Y., Rubenstein, J.L., and Sasai, Y. (2011). Subregional specification of embryonic stem cell-derived ventral telencephalic tissues by timed and combinatory treatment with extrinsic signals. J. Neurosci. 31, 1919–1933.

Driggers, R.W., Ho, C.Y., Korhonen, E.M., Kuivanen, S., Jääskeläinen, A.J., Smura, T., Rosenberg, A., Hill, D.A., DeBiasi, R.L., Vezina, G., et al. (2016). Zika virus infection with prolonged maternal viremia and fetal brain abnormalities. N. Engl. J. Med. Published online March 30, 2016. http://dx.doi.org/10.1056/NEJMoa1601824.

Faria, N.R., Azevedo, R.D., Kraemer, M.U., Souza, R., Cunha, M.S., Hill, S.C., Thézé, J., Bonsall, M.B., Bowden, T.A., Rissanen, I., et al. (2016). Zika virus in

the Americas: Early epidemiological and genetic findings. Science. Published online March 24, 2016. http://dx.doi.org/10.1126/science.aaf5036.

Garcez, P.P., Loiola, E.C., da Costa, R.M., Higa, L.M., Trindade, P., Delvecchio, R., Nascimento, J.M., Brindeiro, R., Tanuri, A., and Rehen, S.K. (2016). Zika virus impairs growth in human neurospheres and brain organoids. Science. Published online April 10, 2016. http://dx.doi.org/10.1126/science.aaf6116.

Goodwin, T.J., Schroeder, W.F., Wolf, D.A., and Moyer, M.P. (1993). Rotating-wall vessel coculture of small intestine as a prelude to tissue modeling: aspects of simulated microgravity. Proc. Soc. Exp. Biol. Med. 202, 181–192.

Haddow, A.D., Schuh, A.J., Yasuda, C.Y., Kasper, M.R., Heang, V., Huy, R., Guzman, H., Tesh, R.B., and Weaver, S.C. (2012). Genetic characterization of Zika virus strains: geographic expansion of the Asian lineage. PLoS Negl. Trop. Dis. 6, e1477.

Hansen, D.V., Lui, J.H., Parker, P.R., and Kriegstein, A.R. (2010). Neurogenic radial glia in the outer subventricular zone of human neocortex. Nature 464, 554–561.

Heymann, D.L., Hodgson, A., Sall, A.A., Freedman, D.O., Staples, J.E., Althabe, F., Baruah, K., Mahmud, G., Kandun, N., Vasconcelos, P.F., et al. (2016). Zika virus and microcephaly: why is this situation a PHEIC? Lancet 387, 719–721.

Jaffe, A.E., Shin, J., Collado-Torres, L., Leek, J.T., Tao, R., Li, C., Gao, Y., Jia, Y., Maher, B.J., Hyde, T.M., et al. (2015). Developmental regulation of human cortex transcription and its clinical relevance at single base resolution. Nat. Neurosci. 18, 154–161.

Jessup, J.M., Goodwin, T.J., and Spaulding, G. (1993). Prospects for use of microgravity-based bioreactors to study three-dimensional host-tumor interactions in human neoplasia. J. Cell. Biochem. 51, 290–300.

Kadoshima, T., Sakaguchi, H., Nakano, T., Soen, M., Ando, S., Eiraku, M., and Sasai, Y. (2013). Self-organization of axial polarity, inside-out layer pattern, and species-specific progenitor dynamics in human ES cell-derived neocortex. Proc. Natl. Acad. Sci. USA 110, 20284–20289.

Kim, J.Y., Liu, C.Y., Zhang, F., Duan, X., Wen, Z., Song, J., Feighery, E., Lu, B., Rujescu, D., St Clair, D., et al. (2012). Interplay between DISC1 and GABA signaling regulates neurogenesis in mice and risk for schizophrenia. Cell 148, 1051–1064.

Kriks, S., Shim, J.W., Piao, J., Ganat, Y.M., Wakeman, D.R., Xie, Z., Carrillo-Reid, L., Auyeung, G., Antonacci, C., Buch, A., et al. (2011). Dopamine neurons derived from human ES cells efficiently engraft in animal models of Parkinson's disease. Nature 480, 547–551.

Kundakovic, M., Gudsnuk, K., Franks, B., Madrid, J., Miller, R.L., Perera, F.P., and Champagne, F.A. (2013). Sex-specific epigenetic disruption and behavioral changes following low-dose in utero bisphenol A exposure. Proc. Natl. Acad. Sci. USA 110, 9956–9961.

Lancaster, M.A., and Knoblich, J.A. (2014). Organogenesis in a dish: modeling development and disease using organoid technologies. Science 345, 1247125.

Lancaster, M.A., Renner, M., Martin, C.A., Wenzel, D., Bicknell, L.S., Hurles, M.E., Homfray, T., Penninger, J.M., Jackson, A.P., and Knoblich, J.A. (2013). Cerebral organoids model human brain development and microcephaly. Nature 501, 373–379.

Lazear, H.M., Govero, J., Smith, A.M., Platt, D.J., Fernandez, E., Miner, J.J., and Diamond, M.S. (2016). A mouse model of Zika virus pathogenesis. Cell Host Microbe. Published online April 5, 2016. http://dx.doi.org/10.1016/j.chom.2016.03.010.

Lui, J.H., Hansen, D.V., and Kriegstein, A.R. (2011). Development and evolution of the human neocortex. Cell 146, 18–36.

Mariani, J., Coppola, G., Zhang, P., Abyzov, A., Provini, L., Tomasini, L., Amenduni, M., Szekely, A., Palejev, D., Wilson, M., et al. (2015). FOXG1-dependent dysregulation of GABA/glutamate neuron differentiation in autism spectrum disorders. Cell 162, 375–390.

Mlakar, J., Korva, M., Tul, N., Popović, M., Poljšak-Prijatelj, M., Mraz, J., Kolenc, M., Resman Rus, K., Vesnaver Vipotnik, T., Fabjan Vodušek, V., et al.

(2016). Zika virus associated with microcephaly. N. Engl. J. Med. *374*, 951–958.

Muguruma, K., Nishiyama, A., Kawakami, H., Hashimoto, K., and Sasai, Y. (2015). Self-organization of polarized cerebellar tissue in 3D culture of human pluripotent stem cells. Cell Rep. *10*, 537–550.

Paşca, A.M., Sloan, S.A., Clarke, L.E., Tian, Y., Makinson, C.D., Huber, N., Kim, C.H., Park, J.Y., O'Rourke, N.A., Nguyen, K.D., et al. (2015). Functional cortical neurons and astrocytes from human pluripotent stem cells in 3D culture. Nat. Methods *12*, 671–678.

Petanjek, Z., Berger, B., and Esclapez, M. (2009). Origins of cortical GABAergic neurons in the cynomolgus monkey. Cereb. Cortex *19*, 249–262.

Pollen, A.A., Nowakowski, T.J., Chen, J., Retallack, H., Sandoval-Espinosa, C., Nicholas, C.R., Shuga, J., Liu, S.J., Oldham, M.C., Diaz, A., et al. (2015). Molecular identity of human outer radial glia during cortical development. Cell *163*, 55–67.

Roost, M.S., van Iperen, L., Ariyurek, Y., Buermans, H.P., Arindrarto, W., De-valla, H.D., Passier, R., Mummery, C.L., Carlotti, F., de Koning, E.J., et al. (2015). KeyGenes, a tool to probe tissue differentiation using a human fetal transcriptional atlas. Stem Cell Reports *4*, 1112–1124.

Tang, H., Hammack, C., Ogden, S.C., Wen, Z., Qian, X., Li, Y., Yao, B., Shin, J., Zhang, F., Lee, E.M., et al. (2016). Zika virus infects human cortical neural pro-

genitors and attenuates their growth. Cell Stem Cell. Published online March 4, 2016. http://dx.doi.org/10.1016/j.stem.2016.02.016.

Thomsen, E.R., Mich, J.K., Yao, Z., Hodge, R.D., Doyle, A.M., Jang, S., She-hata, S.I., Nelson, A.M., Shapovalova, N.V., Levi, B.P., et al. (2015). Fixed single-cell transcriptomic characterization of human radial glial diversity. Nat. Methods *13*, 87–93.

Wang, W., and Lufkin, T. (2000). The murine Otp homeobox gene plays an essential role in the specification of neuronal cell lineages in the developing hypothalamus. Dev. Biol. *227*, 432–449.

Wen, Z., Nguyen, H.N., Guo, Z., Lalli, M.A., Wang, X., Su, Y., Kim, N.S., Yoon, K.J., Shin, J., Zhang, C., et al. (2014). Synaptic dysregulation in a human iPS cell model of mental disorders. Nature *515*, 414–418.

Yin, X., Mead, B.E., Safaee, H., Langer, R., Karp, J.M., and Levy, O. (2016). Engineering Stem Cell Organoids. Cell Stem Cell *18*, 25–38.

Yoon, K.J., Nguyen, H.N., Ursini, G., Zhang, F., Kim, N.S., Wen, Z., Makri, G., Nauen, D., Shin, J.H., Park, Y., et al. (2014). Modeling a genetic risk for schizophrenia in iPSCs and mice reveals neural stem cell deficits associated with adherens junctions and polarity. Cell Stem Cell *15*, 79–91.

Yu, X., and Zecevic, N. (2011). Dorsal radial glial cells have the potential to generate cortical interneurons in human but not in mouse brain. J. Neurosci. *31*, 2413–2420.

Supplemental Figures
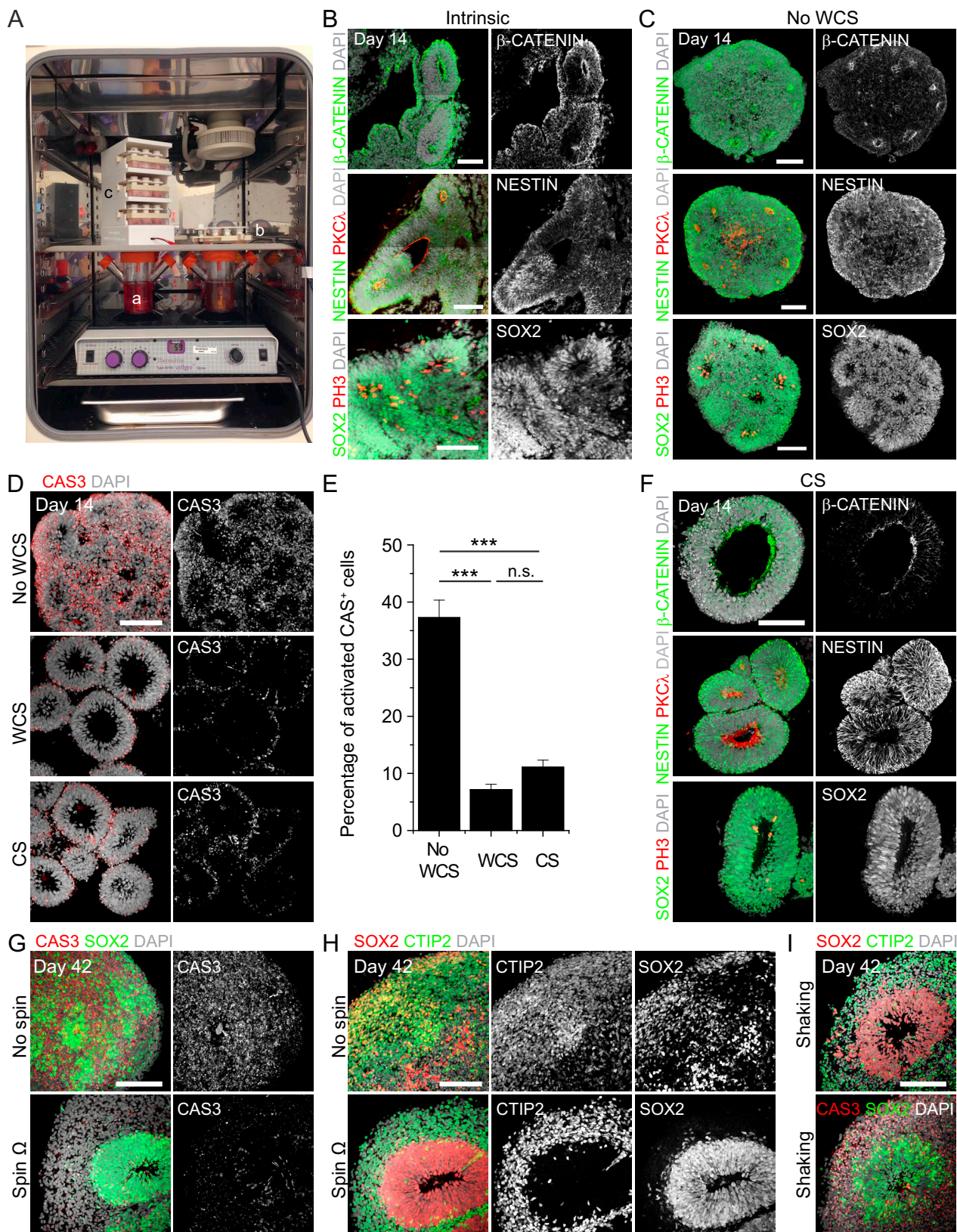
Figure S1. SpinΩ Bioreactor Systems and Culturing Organoids under Different Conditions, Related to Figure 1

(A) A photograph of the incubator showing standard spinning bioreactor system with Corning 125 ml Disposable Spinner Flask and magnetic stirrer plate (a), 12-well version SpinΩ (b), and stackable SpinΩ (c).

(B and C) Sample images of immunostaining of day 14 organoids generated with the "intrinsic protocol" (B, tiling image) and the forebrain protocol without treatment of W (WNT3A), C (CHIR99021) and S (SB-431542) (C). Scale bars: 100 μm.

(D and E) Sample images of immunostaining for apoptosis marker activated-Caspase 3 (CAS3, D) and quantification (E) in organoids generated from different protocols. Scale bar: 100 μm. Values represent mean ± SEM (n = 5 organoids; ***p < 0.0005, Student's t test; n.s, p > 0.05).

(F) Sample images of day 14 organoids generated using the forebrain protocol without WNT3A, showing a similar expression pattern as in Figure 1C. Scale bar: 100 μm.

(G–I) Comparison of forebrain organoids grown in different conditions at day 42. SpinΩ, spinning culture in SpinΩ bioreactor; No spin, stationary culture in an ultra-low attachment plate; Shaking, shaking culture in an ultra-low attachment plate placed on orbital shaker at the same speed as the SpinΩ. Scale bars: 100 μm.
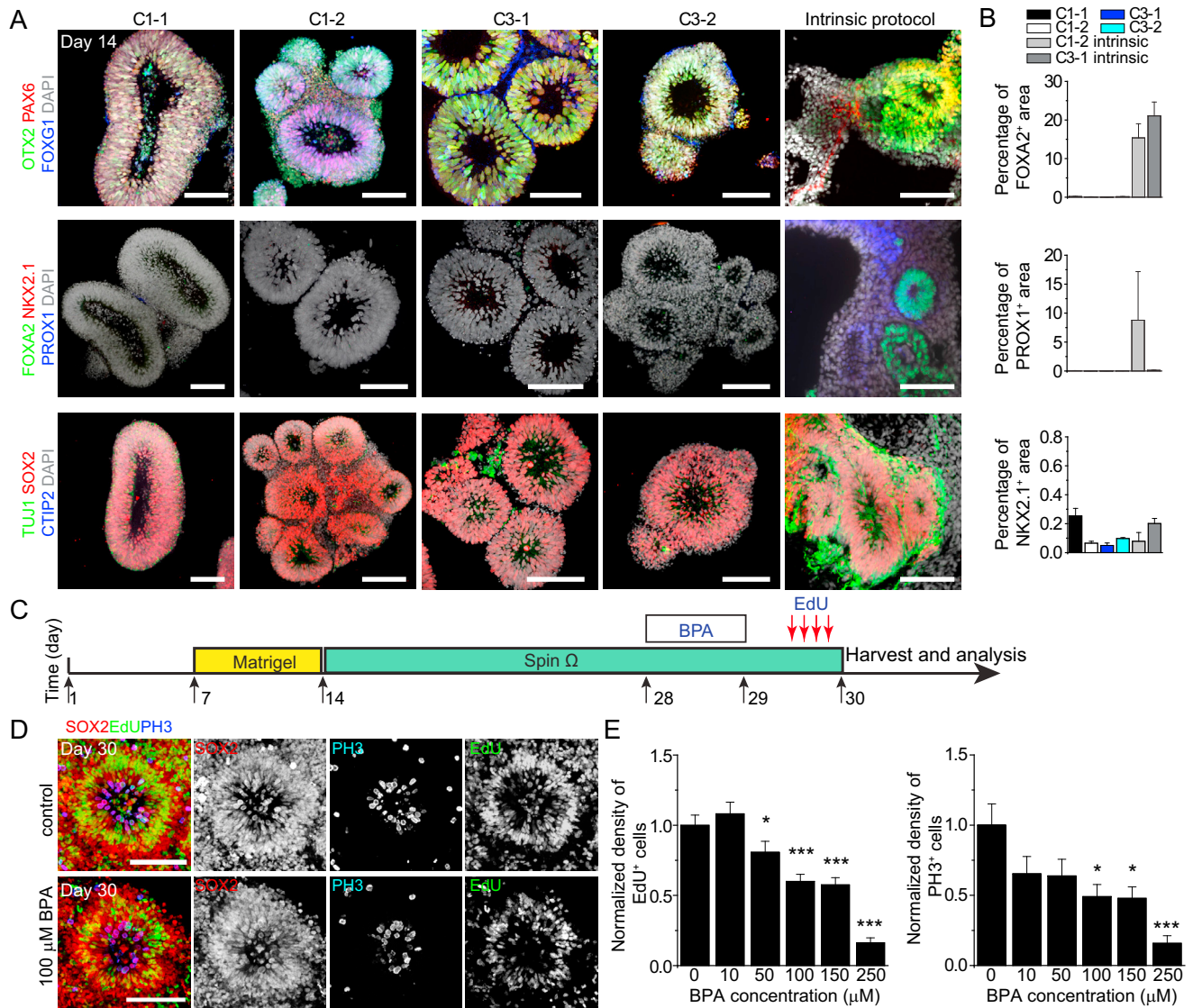
Figure S2. Characterization of Forebrain Organoids from Multiple Human iPSC Lines and Acute Effect of BPA, Related to Figure 2

(A) Sample images of immunostaining of neuroepithelium-like tissues generated using the forebrain and "intrinsic" protocols from multiple human iPSC lines at day 14 for forebrain progenitor markers OTX2, PAX6 and FOXG1 (top panel), and floor plate precursor marker FOXA2, ventral MGE precursor marker NKX2.1, and hippocampal granule cell marker PROX1 (middle panel), and for NPC marker SOX2 and neuronal markers TUJ1 and CTIP2 (bottom panel). Scale bars: 100 μm. Sample images for the "intrinsic protocol" were from tiling multiple images of a large area.

(B) Quantifications of expression of precursor markers from various brain regions at day 14 using forebrain and "intrinsic" protocols. Values represent mean ± SEM (n ≥ 8 organoids each).

(C–E) Effect of acute treatment of forebrain organoids with BPA. Shown in (C) is a schematic diagram for the experimental paradigm. Shown in (D) are sample images of immunostaining of day 30 forebrain organoids for SOX2, PH3 and EdU. Scale bars: 100 μm. Shown in (E) are summaries of quantifications of normalized densities of EdU$^+$ and PH3$^+$ proliferating cells in forebrain organoids treated with different concentrations of BPA. Values represent mean ± SEM (n = 20 cortical structures from at least 8 organoids; *p < 0.05; ***p < 0.0005, Student's t test).
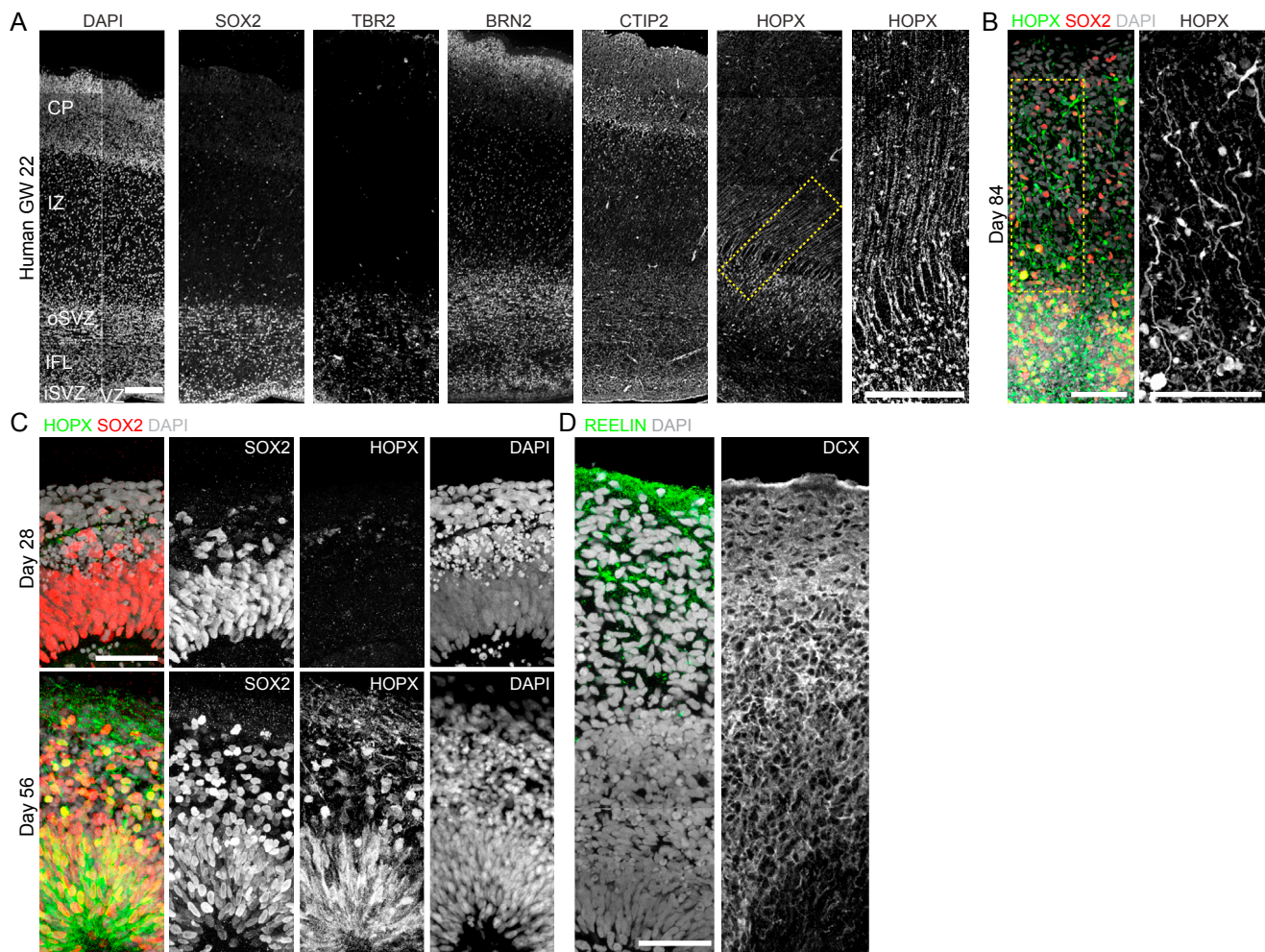
Figure S3. Expression of HOPX in Embryonic Human Cortex and Forebrain Organoids, Related to Figure 3

(A) Sample tiling images of immunostaining of embryonic human cortex at gestational week (GW) 22. Also shown is a magnified view within the dashed line box, revealing HOPX⁺ radial fibers. CP: cortical plate; IZ: intermediate zone; oSVZ: outer subventricular zone; IFL: inner fibrous layer; iSVZ: inner subventricular zone; VZ: ventricular zone. Scale bars: 200 μm.

(B) Sample tiling confocal image showing morphology of SOX2⁺HOPX⁺ cells and their radial processes in a day 84 forebrain organoid. Scale bars: 50 μm.

(C) Sample confocal images of immunostaining for HOPX and SOX2 in day 28 and 56 forebrain organoids. Note that HOPX was absent at day 28 and was expressed in a fraction of SOX2⁺ NPCs in both VZ and SVZ at day 56. Scale bar: 50 μm.

(D) Sample tiling images of immunostaining for Cajal-Retzius cell marker REELIN and neuronal marker DCX at day 84, showing a cell-sparse marginal zone at the pial surface. Scale bar: 50 μm.
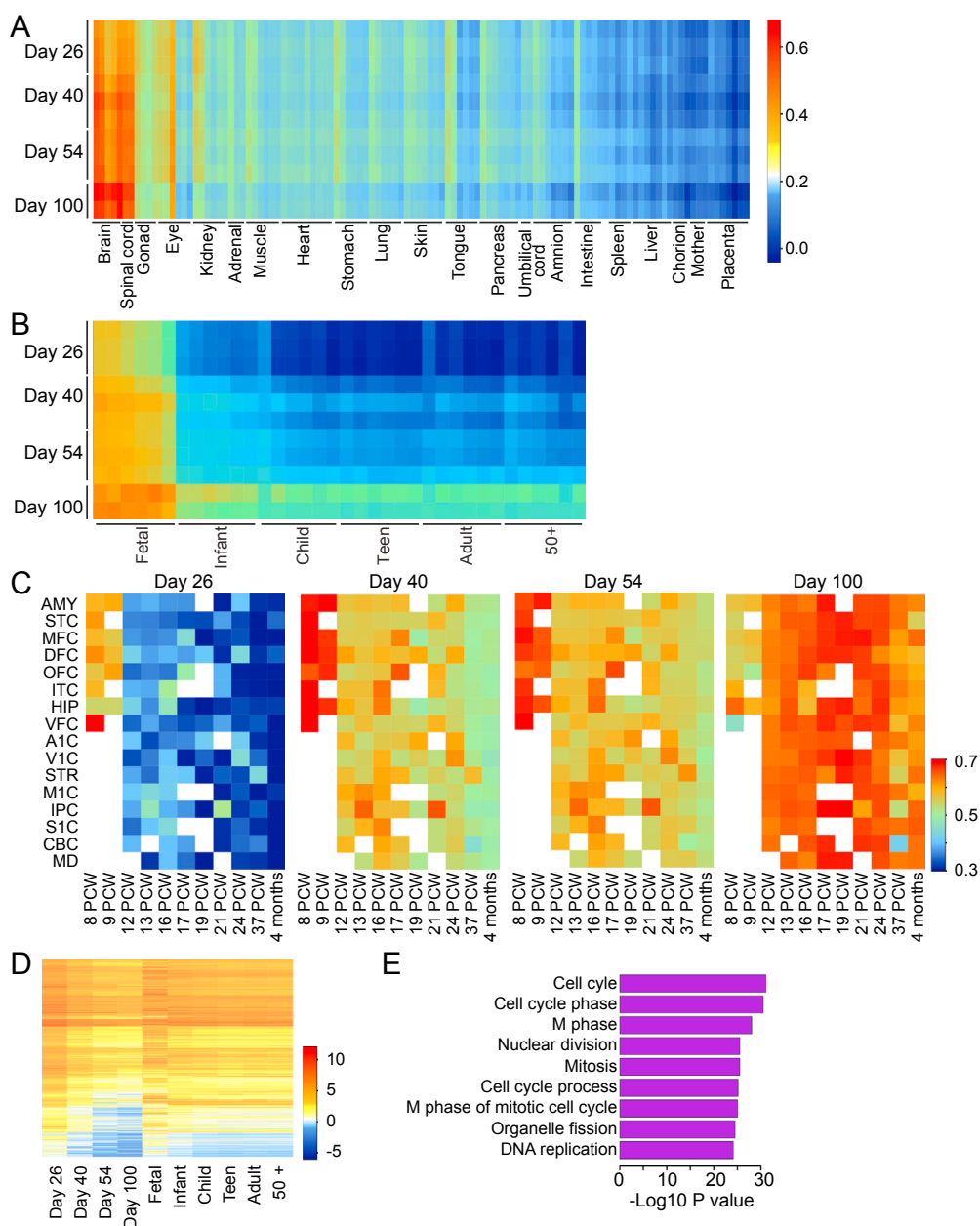
Figure S4. Genome-wide Transcriptome Comparison between Forebrain Organoid and Human Fetal Brain Development, Related to Figure 4

(A) Heatmap of Pearson's correlation analysis of RNA-seq datasets among forebrain organoids at days 26, 40, 54 and 100 and published datasets of 21 different human fetal organs during the first and second trimester (Roost et al., 2015). Individual replicates for Figure 5A are plotted.

(B) Heatmap of Pearson's correlation analysis of RNA-seq datasets among forebrain organoids at different stages and human dorsolateral prefrontal cortex samples across 6 life stages (Jaffe et al., 2015).

(C) Heatmaps of Pearson's correlation analysis of RNA-seq datasets among forebrain organoids at different stages and published transcriptome datasets of 16 different cortical subregions at 10 fetal developmental stages and 1 postnatal stage from Allen Brain Atlas (http://www.brain-map.org/). AMY: amygdaloid complex; STC: posterior (caudal) superior temporal cortex (area 22c); MFC: anterior (rostral) cingulate (medial prefrontal) cortex; DFC: dorsolateral prefrontal cortex; OFC: orbital frontal cortex; ITC: inferolateral temporal cortex (area TEv, area 20); HIP: hippocampus (hippocampal formation); VFC: ventrolateral prefrontal cortex; A1C: primary auditory cortex (core); V1C: primary visual cortex (striate cortex, area V1/17); STR: striatum; M1C: primary motor cortex (area M1, area 4); IPC: posteroventral (inferior) parietal cortex; S1C: primary somatosensory cortex (area S1, areas 3,1,2); CBC: cerebellar cortex; MD: mediodorsal nucleus of thalamus.

(D) Heatmap of gene expression dynamics of downregulated genes between day 26 and later stages of organoid development.

(E) Gene Ontology analysis of downregulated genes by DAVID (Huang da et al., 2009). Nine top terms (in terms of P-values) are shown.
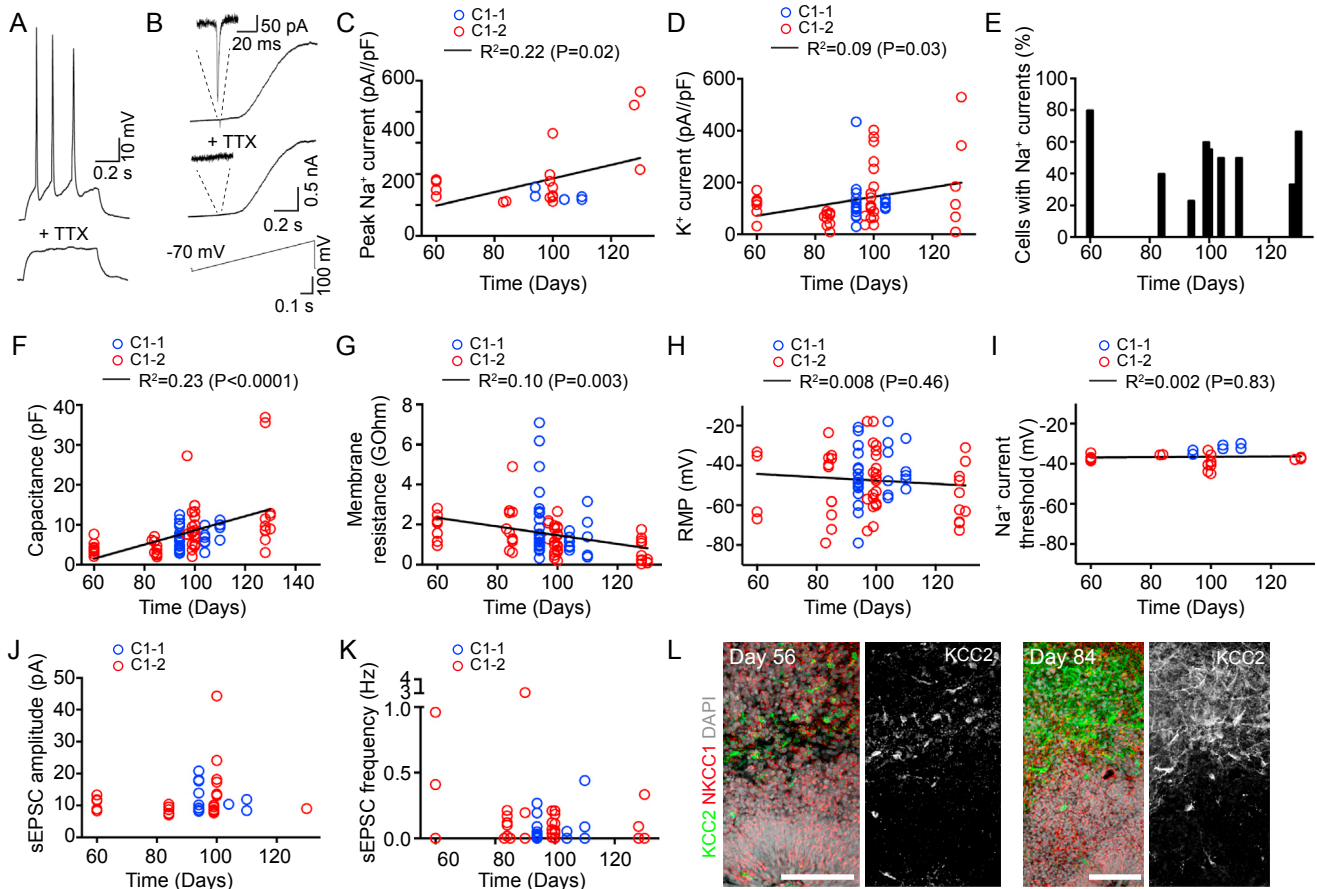
Figure S5. Developmental Properties of Neurons in Forebrain Organoids, Related to Figure 5

(A) Sample current-clamp trace showing a train of action potentials in response to current injection. Bath application of TTX completely blocked the generation of action potentials.

(B) Sample voltage-clamp recording of neurons showing currents in response to a ramp protocol (-90 mV to 110 mV) before and after the application of TTX.

(C and D) Summary plot of increased peak amplitudes of Na$^+$ (C) and K$^+$ (D) currents recorded in organoids over development.

(E) Summary plot showing the percentage of cells in organoids over time that had detectable Na$^+$ currents in response to a voltage ramp protocol (-90 mV to 110 mV).

(F–I) Summary plots showing increased membrane capacitance (F), decreased membrane resistance (G), stable resting membrane potential (H) and threshold for generation of Na$^+$ currents (I) recorded in organoids over development.

(J and K) Plots of sEPSC amplitude (J) and frequency (K) for each neuron recorded in organoids of different ages. The same groups of neurons as shown in Figure 5D (right panel).

(L) Sample images of immunostaining for KCC2 and NKCC1 in day 56 and 84 forebrain organoids. Scale bars: 50 μm.

A — Day 18 | PH3 NESTIN DAPI | PH3 | NESTIN

B — Day 56 | FOXA2 TH DAPI | FOXA2 | TH

Day 56 | TH NURR1 DAPI | NURR1 | TH

Day 56 | DAT TH DAPI | DAT | TH

Day 56 | PITX3 TH DAPI | PITX3 | TH

C — Day 8 | OTP SOX2 DAPI | SOX2 | OTP
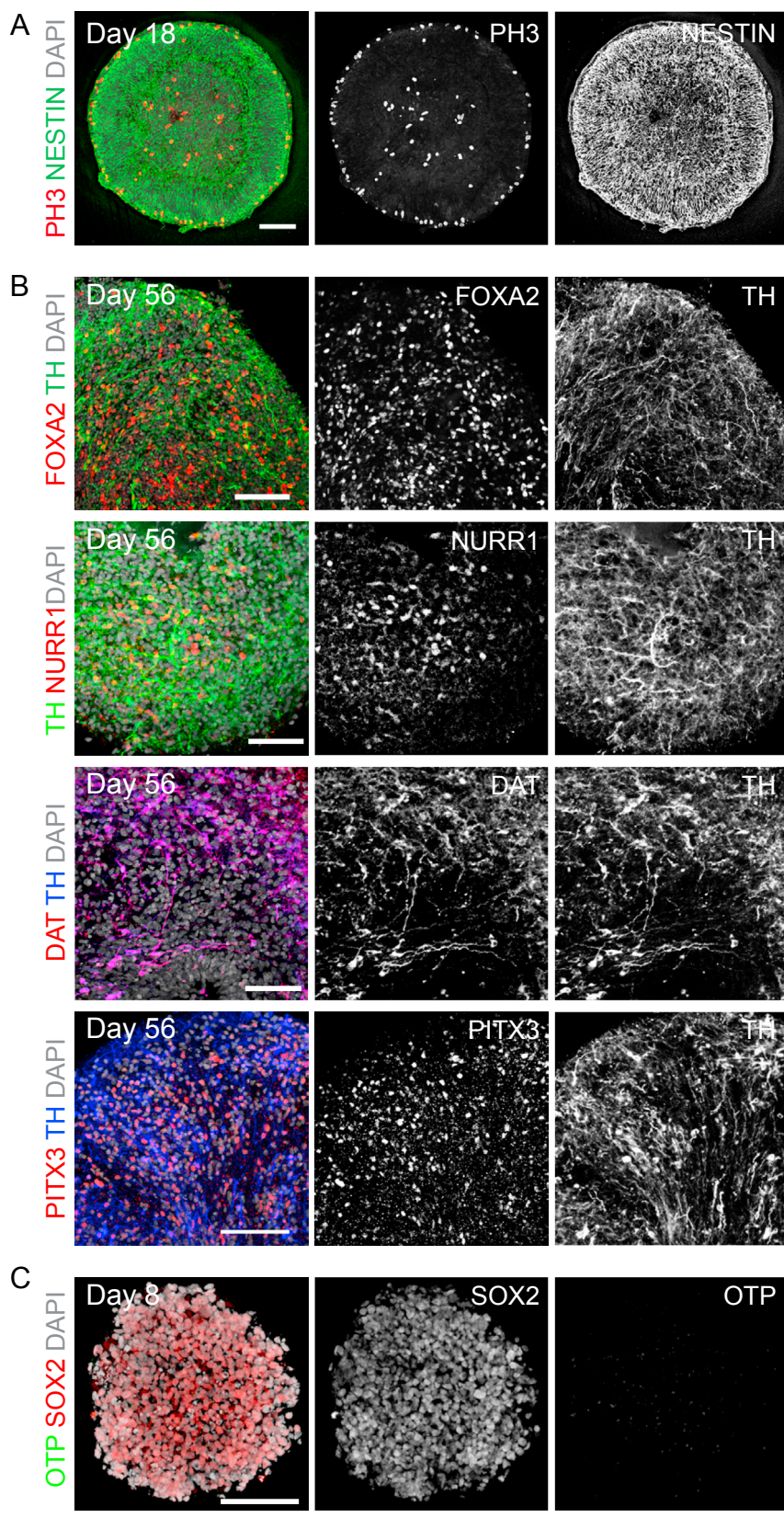
(legend on next page)

Figure S6. Additional Immunohistochemistry Characterization of Midbrain and Hypothalamus Organoids, Related to Figure 6

(A) Sample images of immunostaining for NESTIN and PH3 in day 18 midbrain organoids. Scale bar: 100 μm.

(B) Sample images of immunostaining in day 56 midbrain organoids for DA neuron markers TH, Nuclear receptor related 1 protein (NURR1), PITX3 and dopamine transporter (DAT). Scale bars: 100 μm.

(C) Sample images of immunostaining of a hypothalamus organoid at day 8 showing NPC marker SOX2 and absence of OTP. Scale bar: 100 μm.
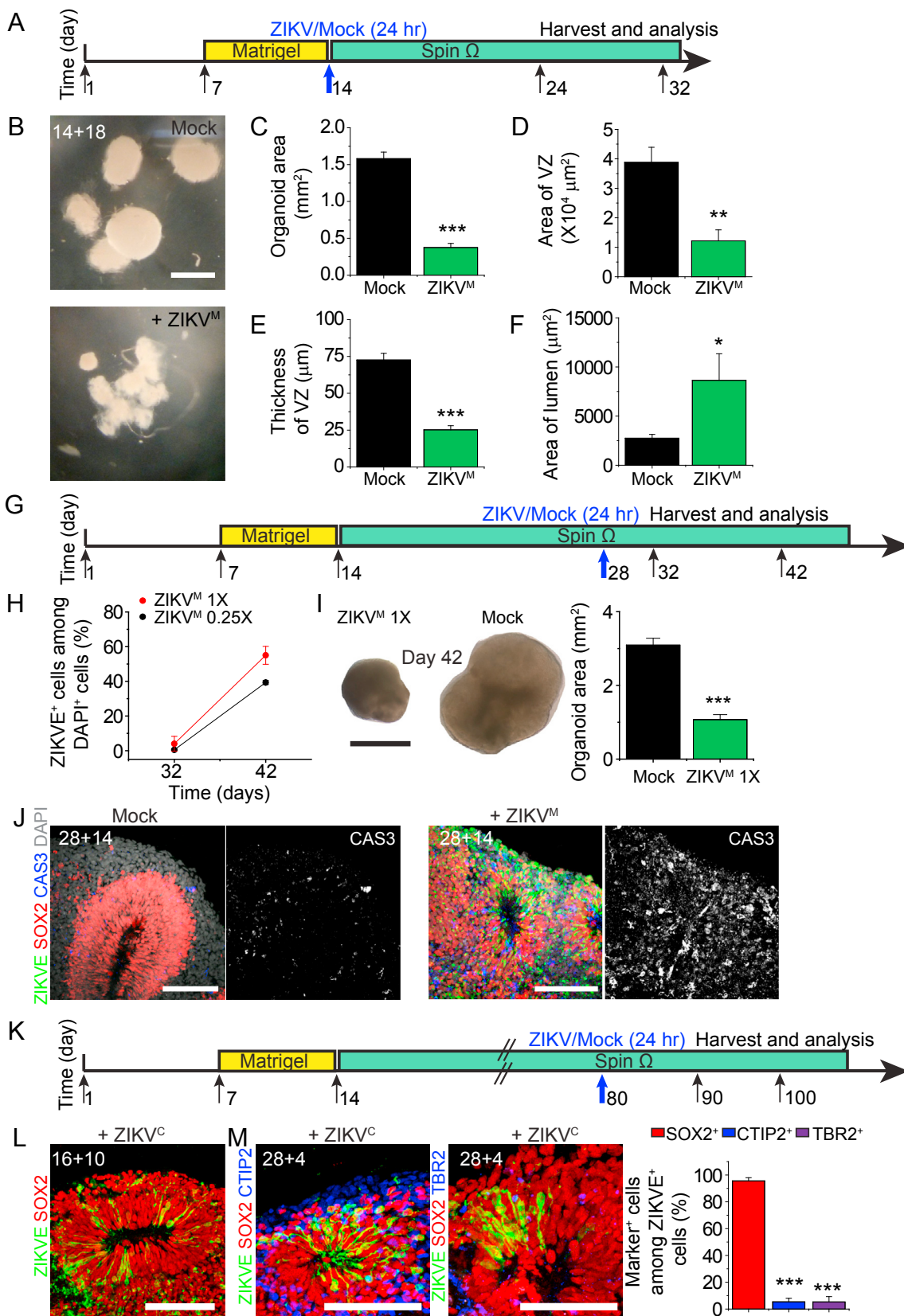
(legend on next page)

Figure S7. Experimental Paradigms and Additional Effects of ZIKV Exposure on Forebrain Organoids, Related to Figure 7

(A–F) Forebrain organoids exposed to ZIKV[M] (1X) or mock-treated at day 14 for 24 hr and analyzed 18 days later (14+18). Shown in (A) is a schematic diagram of the experimental paradigm. Shown in (B-C) are bright-field microscopic images (B) and quantification of the organoid size (C). Scale bar: 1 mm. Also shown are quantifications of VZ area (D), VZ thickness (E) and lumen size (F) measured on immunostained images of organoids under different conditions. Values represent mean ± SEM (n = 5 organoids; ***p < 0.0005, Student's t test).

(G–J) Forebrain organoids exposed to ZIKV[M] (1X or 0.25X) or mock-treated at day 28 for 24 hr and analyzed at day 32 (28+4) or day 42 (28+14). Shown in (G) is a schematic diagram of the experimental paradigm. Shown in (H) is a summary of the percentage of ZIKVE^{+} cells over DAPI in cortical structures at days 32 and 42. Shown in (I) are bright-field microscopic images and quantification of organoid size. Scale bar: 1 mm. Values represent mean ± SEM (n = 6 organoids; ***p < 0.0005, Student's t test). Shown in (J) are sample confocal images of immunostaining for CAS3, SOX2 and ZIKVE. Scale bars: 100 μm.

(K) A schematic diagram for the experimental paradigm for forebrain organoids exposed to ZIKV[M] (1X) at day 80 for 24 hr and analyzed 10 or 20 days later.

(L and M) Sample immunostaining images and quantification of organoids exposed to ZIKV[C] (1X) at day 16 and analyzed 10 days later (16+10; L) or at day 28 and analyzed 4 days later (28+4; M). Scale bars: 100 μm. Values represent mean ± SEM (n = 5 cortical structures from 3 organoids; ***p < 0.0005, Student's t test).

Supplemental Information

Brain-Region-Specific Organoids

Using Mini-bioreactors for Modeling ZIKV Exposure

Xuyu Qian, Ha Nam Nguyen, Mingxi M. Song, Christopher Hadiono, Sarah C. Ogden, Christy Hammack, Bing Yao, Gregory R. Hamersky, Fadi Jacob, Chun Zhong, Ki-jun Yoon, William Jeang, Li Lin, Yujing Li, Jai Thakor, Daniel A. Berg, Ce Zhang, Eunchai Kang, Michael Chickering, David Nauen, Cheng-Ying Ho, Zhexing Wen, Kimberly M. Christian, Pei-Yong Shi, Brady J. Maher, Hao Wu, Peng Jin, Hengli Tang, Hongjun Song, and Guo-li Ming

EXPERIMENTAL PROCEDURES

Bioreactor Design, 3D Printing and Assembling

We used SolidWorks for design and drawings of all parts, including spinning leaf and shafts. Cover units were designed to fit a standard 12-well culture plate (Figure 1A). Autoclavable plate cover and spinning shafts were printed with a 3D printer (Fortus 450mc) using ULTEM 9085, and other parts were printed using polycarbonate. Standalone spinning bioreactors were assembled from parts consisting of IG16 6VDC 051 RPM Gear Motor (SuperDroid Robots TD-060-051), gears (GR.MOLD.SP.M0.5 (US); SDP/SIA 1Z 2MYZ0505206), sleeve bearings (Metric PTFE Sleeve Bearing, for 6 mm Shaft Diameter, 12 mm OD, 10 mm Length; McMaster-Carr 2685T11), Aluminum Unthreaded Spacers (1/4" OD, 3/4" Length, #4 Screw Size; McMaster-Carr 92510A308), and a power supply (Hosa Cable ACD477 Universal AC Power Supply; Amazon). The modular individual bioreactors were made to fit into a stackable bioreactor with some modifications (Figure S1Ac). All gears in the stackable bioreactor were driven by motor with higher output (IG32 Right Angle 12VDC 043 RPM Gear Motor; SuperDroid Robots TD-035-043) connected to a series of shaft couplings (Rigid, Setscrew; Misumi CPR16-6-6), rotary shafts (D Cut; Misumi SSFRV6-55-F19-T12), bearings (Single Row, Metric Sizes, Acetal Plastic Radial Ball Bearings fitted with Glass Balls; KMS Bearings A626-G), and gears (Module 0.5, 96 Teeth, 20° Pressure Angle, Acetal/Brass Insert Spur Gear (SDP/SIA 1Z 2MYZ0509606). The blueprints for 3D printing of the 12-well version and the stackable version of the bioreactor are provided in Data S1. Each folder contains the CAD files for design of the bioreactor components as well as a PDF reference file to view full assembly of the pieces.

Maintenance of Human iPSCs

Human iPSC lines used in the current study were previously fully characterized (Wen et al., 2014; Yoon et al., 2014). They were cultured in stem cell medium, consisting of DMEM:F12 (Invitrogen) supplemented with 20% Knockout Serum Replacer (Gibco), 1X Non-essential Amino Acids

(Invitrogen), 1X Penicillin/Streptomycin (Invitrogen), 1X 2-Mercaptoenthanol (Millipore), 1X

Glutamax (Invitrogen), and 10 ng/ml FGF-2 (Peprotech) as previously described (Yoon et al.,

2014). Culture medium was changed every day. Human iPSCs were passaged every week onto a

new plate pre-seeded with irradiated CF1 mouse embryonic fibroblasts (Charles River). iPSCs were

detached from the plate by treatment of 1 mg/ml Collagenase Type IV (Invitrogen) for 1 hr. iPSC

colonies were further dissociated into smaller pieces by manual pipetting. All studies were

performed with approved protocols of Johns Hopkins University School of Medicine.

Culture of Forebrain Organoids from Human iPSCs

To generate forebrain-specific organoids (Figure 1B), human iPSC colonies were detached 7 days

after passage with Collagenase Type IV, washed with fresh stem cell medium and cultured in a 15

ml conical tube. On day 1, detached and washed iPSC colonies were transferred to an Ultra-Low

attachment 6-well plate (Corning Costar), containing 3 ml of stem cell medium (without FGF-2), plus

2 μM Dorsomorphine (Sigma) and 2 μM A83-01 (Tocris). On days 5-6, half of the medium was

replaced with induction medium consisting of DMEM:F12, 1X N2 Supplement (Invitrogen), 10 μg/ml

Heparin (Sigma), 1X Penicillin/Streptomycin, 1X Non-essential Amino Acids, 1X Glutamax, 4 ng/ml

WNT-3A (R&D Systems), 1 μM CHIR99021 (Cellagentech), and 1 μM SB-431542 (Cellagentech).

On day 7, organoids were embedded in Matrigel (BD Biosciences) and continued to grow in

induction medium for 6 more days. On day 14, embedded organoids were mechanically dissociated

from Matrigel by pipetting up and down onto the plate with a 5 ml pipette tip. Typically, 10 - 20

organoids were transferred to each well of a 12-well spinning bioreactor (SpinΩ) containing

differentiation medium, consisting of DMEM:F12, 1X N2 and B27 Supplements (Invitrogen), 1X

Penicillin/Streptomycin, 1X 2-Mercaptoenthanol, 1X Non-essential Amino Acids, 2.5 μg/ml Insulin

(Sigma). At day 71, differentiation medium was exchanged with maturation medium, consisting of

Neurobasal (Gibco), 1X B27 Supplement, 1X Penicillin/Streptomycin, 1X 2-Mercaptoenthanol, 0.2

mM Ascorbic Acid, 20 ng/ml BDNF (Peprotech), 20 ng/ml GDNF (Peprotech), 1 ng/ml TFGβ

(Peprotech), and 0.5 mM cAMP (Sigma). The organoids could grow beyond 110 days in maturation medium. All media were changed every other day. For the stationary culture, day 14 organoids were generated following the same protocol and then maintained in an Ultra-Low attachment 6 well plate (Corning Costar) with differentiation media. The "intrinsic protocol" for differentiation of human iPSCs into cerebral organoids followed the published protocol (Lancaster et al., 2013).

Culture of Midbrain Organoids from Human iPSCs

To generate midbrain-specific organoids (Figure 6A), human iPSC colonies were detached with Collagenase Type IV 7 days after passage and washed with fresh stem cell medium in a 15 ml conical tube. On day 1, the detached and washed iPSC colonies were transferred to an Ultra-Low attachment 6-well plate containing EB medium, consisting of DMEM:F12, 15% Knockout Serum Replacer, 1X Glutamax, 1X 2-Mercaptoenthanol, 100 nM LDN-193189, 10 μM SB-431542, 100 ng/ml SHH (Peprotech), 2 μM Purmorphamine (Stemgent), 100 ng/ml FGF-8 (Peprotech). On day 5, EB medium was gradually switched to SHH medium, consisting of DMEM:F12, 1X N2 Supplement, 1X Glutamax, 100 nM LDN-193189, 3 μM CHIR99021, 100 ng/ml SHH, 2 μM Purmorphamine, 100 ng/ml FGF-8. On day 7, SHH medium was replaced with induction medium, consisting of DMEM:F12, 1X N2 Supplement, 1X Glutamax, 100 nM LDN-193189, 3 μM CHIR99021. On day 14, 10-20 organoids were transferred to SpinΩ with differentiation medium, consisting of Neurobasal, 1X B27 Supplement, 1X Glutamax, 1X 2-Mercaptoenthanol, 20 ng/ml BDNF, 20 ng/ml GDNF, 0.2 mM Ascorbic Acid, 1 ng/ml TGFβ, and 0.5 mM c-AMP. All media were changed every other day.

Culture of Hypothalamus Organoids from Human iPSCs

To generate hypothalamus-specific organoids (Figure 6F), human iPSC colonies were detached 7 days following passaging with Collagenase Type IV, and washed with fresh stem cell medium in a 15 ml conical tube. On day 1, detached and washed iPSC colonies were transferred to an Ultra-

Low attachment 6-well plate (Corning Costar) containing stem cell medium. One day after (day 2), stem cell medium was replaced with induction medium A, consisting of DMEM:F12, 10% Knockout Serum Replacer, 1X Non-essential Amino Acids, 1X Penicillin/Streptomycin, 1X 2-Mercaptoenthanol, 1X Glutamax, 2.5 μM LDN-193189 (Stemgent), 3 μM SB-431542, and 450 μM 1-Thioglycerol (Sigma). On day 4, the medium was switched to induction medium B, consisting of DMEM:F12, 10% Knockout Serum Replacer, 1X Non-essential Amino Acids, 1X Penicillin/Streptomycin, 1X Glutamax, 1X N2 Supplement, 10 ng/m Wnt-3A, 20 ng/ml SHH, and 2 μM Purmorphamine. On day 7, 5-10 organoids were transferred to a 12-well spin bioreactor and induction medium B was replaced with differentiation medium, consisting of DMEM:F12/Neurobasal (1:1 ratio), 1X B27 Supplement, 1X Non-essential Amino Acids, 1X Penicillin/Streptomycin, 1X Glutamax, 10 ng/ml FGF-2 and 10 ng/ml CTNF (Peprotech). Media were changed every other day.

Tissue Preparation and Immunohistochemistry

Whole organoids were fixed in 4% Paraformaldehyde in Phosphate Buffered Saline (BPS) for 30-60 min at room temperature. Organoids were washed 3 times with PBS and then incubated in 30% sucrose solution overnight. Organoids were embedded in tissue freezing medium (General Data) and sectioned with a cryostat (Leica). For immunostaining, freezing medium was washed with PBS before permeablization with 0.2% Triton-X in PBS for 1 hr. Tissues were blocked with blocking medium consisting of 10% donkey serum in PBS with 0.1% Tween-20 (PBST) for 30 min. Primary antibodies diluted in blocking solution were applied to the sections overnight at 4°C. After washing with PBST, secondary antibodies diluted in blocking solution were applied to the sections for 1 hr at room temperature. Finally, sections were washed with PBST and stained with DAPI. All images were captured by a confocal microscope (Zeiss LSM 700). For paraffin-embedded human samples, slides were first deparaffinized and retrieved using sodium citrate heated to boil in a microwave oven and immunostained as above. See list of antibodies and their information in Table S1. Some

sample images shown were from tiling multiple images of a large area as indicated in figure legends.

BPA Treatment Experiment

Forebrain organoids were grown using the protocol described above. For the long-term BPA treatment experiment (Figure 2E-F), forebrain organoids at day 14 from the same batch were distributed randomly into separate wells within SpinΩ and treated with different concentrations of BPA (Sigma). BPA was dissolved in sequential dilutions in differentiation media with 0.05% methanol, which was also added in the control condition. Media containing BPA was replaced every other day until analysis on day 28. A previous study determined that tissue culture plates do not contain detectable BPA (Biswanger et al., 2006). Quantification was conducted by investigators blind to culture conditions.

For the acute BPA treatment experiment (Figure S2C-E), forebrain organoids were grown to day 28 and treated with corresponding concentrations of BPA for 24 hr. At day 29, the culture media was replaced with fresh media and washed 3 times to remove residual BPA. Organoids were then pulsed with 10 µM EdU for 2 hr. The media was then replaced and organoids were washed 3 times with fresh media. At day 30, organoids were fixed for immunohistochemistry and EdU detection using Click-iT® EdU Alexa Fluor® 488 Imaging Kit (ThermoFisher C10337) according to the manufacturer's manual, followed by immunostaining for SOX2 and PH3. Images were acquired with a Zeiss LSM 700 Confocal system at 25x magnification. Quantification was performed by counting the number of EdU and PH3$^+$ nuclei within SOX2$^+$ ventricular structures that were defined by neural tube-like morphology. EdU and PH3 densities were normalized to the area of ventricular structures measured in ImageJ software. Quantification was conducted by investigators blind to culture conditions.

Quantification of Cell Fates and Layer Thickness

For cell fate quantifications (Figure 2A and S2A-B), organoids grown from the "intrinsic protocol" and forebrain protocol were immunostained for SOX2, PAX6 and OTX2 at day 14. Images were acquired with a Zeiss Axiovert 200M fluorescent microscope. Neural tube structures were counted as positive for forebrain markers when more than 80% of all nuclei were positive for respective markers. Markers for different brain regions (FOXA2, NKX2.1 and PROX1) were quantified by measuring the area stained positive for markers and normalized to DAPI in ImageJ software.

Organoids grown from the "intrinsic protocol" and forebrain protocol were immunostained for SOX2, TUJ1 and CTIP2 at days 14 and 28. The ventricular-like zone (VZ) was defined by SOX2 immunoreactivity and neural-tube morphology and the outer layer was defined by the area outside the VZ to the nearest pial surface. For each ventricular structure, 3 measurements were performed forming a right angle fan area pointing to the nearest pial surface, at 0, 45 and 90 degrees (Figure 2B, upper panel). The length for VZ and outer layer was measured in ImageJ software. The relative VZ thickness was defined as the ratio of VZ thickness to VZ plus outer layer thickness. Layer thickness measurements at days 56 and 84 in forebrain organoids were performed similarly as described above with the addition of SVZ (Figure 3M, upper panel). The SVZ was defined by the region within a mixed population of SOX2$^+$ and CTIP2$^+$ nuclei outside the VZ. The cortical plate (CP) was defined by the region from the boundary of SVZ to the pial surface within exclusive CTIP2$^+$ nuclei. Relative thicknesses for VZ, SVZ and CP were calculated by the ratio to total thickness from ventricular to pial surface.

RNA-Seq and Bioinformatics Analyses

Forebrain organoids at days 26, 40, 54 and 100 (three samples for the first three time points and two samples for day 100) were collected and processed for RNA-seq and bioinformatics analyses as previously described (Tang et al., 2016).

Sequence read counts for 22 different human fetal organs (Figure 4A) were obtained from GSE66302. The sequences were aligned to UCSC hg19 reference genome using tophat v2.0.13

(Trapnell et al., 2012), and the read counts were obtained using R/Bioconductor (Gentleman et al., 2004). Human dorsolateral prefrontal cortex RNA-seq datasets (RPKM values) from six different life stages were obtained from (Jaffe et al., 2015) (http://www.nature.com/neuro/journal/v18/n1/extref/nn.3898-S9.zip). RNA-seq gene expression (RPKM) for 11 time points of fetal development and 16 different brain regions were obtained from Allen Brain Atlas (http://www.brain-map.org/). All gene expression values are summarized as the log RPKM values against the Ensembl gene annotation.

To quantify gene expression correlation between organoids from the current study and fetal organs (Figure 4A), we first selected genes with moderately high average expression levels and variance. Briefly, we only used genes with average expression levels greater than three and variance greater than one from fetal organs. These genes show marked differences among organs and thus are more informative than using all genes in the correlation analysis. Pearson correlations were computed based on expression of these genes. Correlations were averaged for biological replicates in Figure 4A. Figure S4A shows all the correlation values. We found that the patterns of correlation were stable against the gene selection criteria. Thresholds used for selecting genes, albeit arbitrary, had very little impact on the final results. The same strategy was used to compute the correlations between organoid and other samples (brains at different developmental stages and regions).

Differentially expressed genes between day 26 and late stages of organoids were defined as genes with absolute log fold changes of RPKM greater than one, and average baseline expression (log RPKM) greater than 2 (Table S2 and Figure 4C). Schizophrenia-related risk genes were obtained from Schizophrenia Gene Resource (SZGR) (http://bioinfo.mc.vanderbilt.edu/SZGR/). Autism-related risk genes were obtained from Simons Foundation Autism Research Initiative (SFARI) (https://gene.sfari.org/autdb/HG_Home.do). The significance of gene overlap was assessed by chi-squared test on 2-by-2 tables.

R programming language was used to perform all data analysis and generate the figures.

Electroporation

Organoids at day 50 were transferred into Petri dishes containing PBS, and 2 μl of GFP expressing plasmid (pCAGGS-eGFP, 2 μg/μl, diluted in sterile PBS with 0.01% fast green) was injected into 3-4 locations within an organoid using a beveled and calibrated micropipette. Five pulses (40 V, 50 ms in duration with a 950 ms interval) were delivered with tweezer electrodes (CUY650-5, Nepa Gene) by a CUY21SC electroporator (Nepa Gene) as previously described (Yoon et al., 2014). Electroporated organoids were transferred back to SpinΩ and cultured until fixation.

Electrophysiology

Organoid slices were prepared by embedding organoids in 4% low melting point agarose cooled to approximately 32°C. Slices (250 µm) were sectioned using a vibratome (Microm HM650V) and stored at room temperature, oxygenated (95% O_2, 5% CO_2) artificial cerebrospinal fluid (ACSF) containing (in mM): 125 NaCl, 25 $NaHCO_3$, 1.25 NaH_2PO_4, 3 KCl, 25 dextrose, 1 $MgCl_2$, and 2 $CaCl_2$, pH 7.3. Slices were immediately ready for recording.

ACSF was oxygenated (95% O_2, 5% CO_2) and bath temperature was approximately 38°C. Patch pipettes were fabricated from borosilicate glass (N51A, King Precision Glass, Inc.) to a resistance of 2-5 MΩ. For current- and voltage-clamp measurements, pipettes were filled with (in mM): 125 potassium gluconate, 10 HEPES, 4 Mg-ATP, 0.3 Na-GTP, 0.1 EGTA, 10 phosophocreatine, 0.05%, adjusted to pH 7.3 with KOH. For all experiments (except Figure 6H), $GABA_A$ receptors were blocked with SR-95531 (Gabazine, 5 µM, Abcam). In sEPSC experiments, synaptic currents were blocked with 6,7-Dinitroquinoxaline-2,3-dione (DNQX, 10µM, Abcam). Sodium currents and action potentials were blocked with tetrodotoxin (TTX, 300 nM, Abcam). Current signals were recorded with either an Axopatch 200B (Molecular Devices) or a Multiclamp 700A amplifier (Molecular Devices) and were filtered at 2 kHz using a built in Bessel filter and digitized at 10 kHz. Voltage signals were filtered at 2 kHz and digitized at 10kHz. Data were

acquired using Axograph on a Dell PC (Windows 7). For voltage clamp recordings, cells were held at -70 mV.

Calcium Imaging Analysis

Calcium imaging was performed similarly to previous descriptions (Kim et al., 2012). Organoids were loaded with Fluo-4 (Life Technologies) for 30 min before the start of imaging. Throughout experiments, oxygenated aCSF was continuously perfused at a rate of 3 ml/min at room temperature (25 ± 2°C). Glutamate and GABA were added to media during imaging sessions at a final concentration of 20 μM and 10 μM, respectively. Bicuculline was added by bath application to media during imaging at a final concentration of 50 μM and imaging was resumed after a 15-min incubation time. Cells were excited at 488 nm, and Fluo-4 signal was collected at 505–550 nm. Images were acquired and analyzed using NIH Image J software. The Ca^{2+} signal change was determined by ΔF/F [ΔF/F = [(F1-B1)-(F0-B0)]/(F0-B0)], which was normalized to the mean fluorescence intensity measured at the baseline condition (set as 0%).

Modeling ZIKV Exposure

ZIKV was prepared and titered as previously described (Tang et al., 2016). Supernatant from $ZIKV^M$ infected mosquito C6/36 or $ZIKV^C$ infected Vero cells was diluted 1:10 (1X) or 1:40 (0.25X) into forebrain organoid differentiation media, and applied directly to forebrain organoids in SpinΩ. The virus inoculum was removed after a 24 hour incubation in spinning culture and replaced with fresh medium. Forebrain organoids infected at day 28 were pulsed with 10 μM EdU for 2 hours on day 42, and fixed for analysis 24 hours later. Quantitative analyses were conducted on randomly selected cortical structures captured by confocal microscope (Zeiss LSM 700). Cell proliferation was measured by density of PH3^{+} or EdU[+] nuclei in ventricular structures similar to those described in BPA experiments. Cell death was quantified by counting activated caspase-3[+] nuclei over total nuclei stained by DAPI. Area of VZ and lumen, and thickness of VZ and neuronal layers were

measured using ImageJ software. Overall size of organoids was measured under a calibrated 4X

bright field microscope.

REFERENCES

Biswanger, C., Davis, L., and Roberts, R.A. (2006). Estrogenic impurities in tissue culture plastic ware are not bisphenol A. In Vitro Cellular & Developmental Biology - Animal *42*, 294-297.

Gentleman, R.C., Carey, V.J., Bates, D.M., Bolstad, B., Dettling, M., Dudoit, S., Ellis, B., Gautier, L., Ge, Y., Gentry, J.*, et al.* (2004). Bioconductor: open software development for computational biology and bioinformatics. Genome biology *5*, R80.

Jaffe, A.E., Shin, J., Collado-Torres, L., Leek, J.T., Tao, R., Li, C., Gao, Y., Jia, Y., Maher, B.J., Hyde, T.M.*, et al.* (2015). Developmental regulation of human cortex transcription and its clinical relevance at single base resolution. Nat Neurosci *18*, 154-161.

Kim, J.Y., Liu, C.Y., Zhang, F., Duan, X., Wen, Z., Song, J., Feighery, E., Lu, B., Rujescu, D., St Clair, D.*, et al.* (2012). Interplay between DISC1 and GABA signaling regulates neurogenesis in mice and risk for schizophrenia. Cell *148*, 1051-1064.

Lancaster, M.A., Renner, M., Martin, C.A., Wenzel, D., Bicknell, L.S., Hurles, M.E., Homfray, T., Penninger, J.M., Jackson, A.P., and Knoblich, J.A. (2013). Cerebral organoids model human brain development and microcephaly. Nature *501*, 373-379.

Tang, H., Hammack, C., Ogden, S.C., Wen, Z., Qian, X., Li, Y., Yao, B., Shin, J., Zhang, F., Lee, E.M.*, et al.* (2016). Zika Virus Infects Human Cortical Neural Progenitors and Attenuates Their Growth. Cell Stem Cell.

Trapnell, C., Roberts, A., Goff, L., Pertea, G., Kim, D., Kelley, D.R., Pimentel, H., Salzberg, S.L., Rinn, J.L., and Pachter, L. (2012). Differential gene and transcript expression analysis of RNA-seq experiments with TopHat and Cufflinks. Nat Protoc *7*, 562-578.

Wen, Z., Nguyen, H.N., Guo, Z., Lalli, M.A., Wang, X., Su, Y., Kim, N.S., Yoon, K.J., Shin, J., Zhang, C.*, et al.* (2014). Synaptic dysregulation in a human iPS cell model of mental disorders. Nature *515*, 414-418.

Yoon, K.J., Nguyen, H.N., Ursini, G., Zhang, F., Kim, N.S., Wen, Z., Makri, G., Nauen, D., Shin, J.H., Park, Y.*, et al.* (2014). Modeling a genetic risk for schizophrenia in iPSCs and mice reveals neural stem cell deficits associated with adherens junctions and polarity. Cell Stem Cell *15*, 79-91.